

### Potassium dependent structural changes in the selectivity filter of HERG potassium channels



**Open Access** This file is licensed under a Creative Commons Attribution 4.0

International License, which permits use, sharing, adaptation, distribution and reproduction in any medium or format, as long as you give appropriate credit to

the original author(s) and the source, provide a link to the Creative Commons license, and indicate if changes were made. In the cases where the authors are anonymous, such as is the case for the reports of anonymous peer reviewers, author attribution should be to 'Anonymous Referee' followed by a clear attribution to the source work. The images or other third party material in this file are included in the article's Creative Commons license, unless indicated otherwise in a credit line to the material. If material is not included in the article's Creative Commons license and your intended use is not permitted by statutory regulation or exceeds the permitted use, you will need to obtain permission directly from the copyright holder. To view a copy of this license, visit <http://creativecommons.org/licenses/by/4.0/>.

## REVIEWER COMMENTS

Reviewer #1 (Remarks to the Author):

The authors investigate a novel mechanism for HERG inactivation at the selectivity filter (C-type) by combining a novel HERG structure in very low K with MD simulation and mutagenesis analyses. In contrast to prior publications (Wang 2017 Cell, Li 2021 Sci Adv, Bassetto 2023 Nat Comm) that focus on a constriction between S1 and S2 caused by rearrangement of the uniquely displaced F627 residue, the evidence from the low K structure here points to the flipping of the V625 carbonyl oxygen out of the conduction path, leading to imperiled K transport due to a constriction between S3 and S4. Overall, the methods and data presented appear to be robust, and consistent with a novel mechanism activated in the low-K conditions. My concerns for this putative mechanism are that (1) it is derived primarily from simulations, whereas some prior experimental evidence suggests that it may be incorrect or need better explanation (see point 1 below), and (2) it is derived from the low-K condition, which may overlap voltage-dependent C-type inactivation but may point to a separate mechanism. Therefore, though I think this mechanism is plausible, the evidence presented here suggests that it may contribute to low-K inactivation rather than the primary driver of voltage-dependent HERG C-type inactivation.

1. The mechanism demonstrated here seems to me inconsistent with prior experimental evidence showing enhanced (negatively-shifted) voltage-dependent inactivation of the Y616F mutant (Supp Fig 2, Kopfer Plos ONE 2012). A key point of the putative V625 mechanism is that S620 switches from binding G626 to V625 during inactivation, stabilizing the inactive conformation. For this to happen, there is a transient period of S620-Y616 binding, to lower the energy barrier for V625 flipping. Thus, mutating Y616 should prevent inactivation, which the authors point out is consistent with non-inactivating Y616L mutants in Bassetto 2023. However, Y616 is shown to be a critical part of the activation pathway in that paper, and a substantial mutation such as Y616L appears to alter activation profoundly as well. This suggests that the Y616L mutant is likely altering the SF structure more globally and the effects on inactivation may not be specific to any particular mechanism. In contrast, the Y616F mutant studied in Kopfer is much more conservative, better maintaining the hydrophobic interactions that drive activation, but abolishing the hydrogen bonding that appears to be critical for the mechanism proposed here. This mutant would also be expected to distinguish between the V625 mechanism proposed here and the F627-Y616-N629 inactivation mechanism proposed by Li 2021 Sci Adv. In that paper, Y616-N629 bonding stabilizes the open conformation, whereas Y616-S620 interaction drives inactivation in the mechanism proposed here. If my understanding is correct, one would expect Y616F to enhance inactivation if the Li mechanism prevails, whereas it should abolish inactivation if the V625 mechanism proposed here is more important. Critically, Y616F appears to significantly enhance, rather than abolish, inactivation, and thus appears to suggest the F627 rearrangements are the critical factor. The authors would need to repeat the Y616F electrophysiology experiments to show different results (perhaps using different K concentrations to find a condition of abolished inactivation), or provide a different explanation (or what I may be missing in my interpretation), to reconcile this seemingly fundamental inconsistency. Nevertheless, to me this appears to suggest that the mechanism proposed here is less important for canonical HERG inactivation.

2. The structural work is intriguing in showing that the majority of rearrangement between high and low K structures to be centered on the selectivity filter. Given that they analyzed a large number of particles, Cryosparc 4.0 3D classification without alignment may resolve intermediate low-occupancy states that may help bolster the mechanism proposed.

3. The electrophysiology data is poorly annotated. Methods say that both high and low K conditions were used, but this is not labelled nor described in the text. Y axis scale bars are missing.

4. For ease of understanding for a broader audience, it would be useful to label all the relevant figures (e.g. Fig. 1D, E, 2B, 3A, 4A, 6) with both S0-S4 as well as critical residues V625, F627, etc. This would make it much easier to understand which part of the selectivity filter is being diagrammed in each panel rather than having to jump back and forth between S0-S4 labelled panels and amino-acid labelled panels.

Reviewer #2 (Remarks to the Author):

This manuscript by Lau et al. describes new insights into the rapid hERG inactivation process underlying this channel's key role in ventricular repolarization. Exploiting the K sensitivity characteristic of C-type inactivation to bias conformation toward the open or inactivated state, the authors used cryo-EM, electrophysiology, and molecular dynamics (MD) simulations to present a convincing picture of the underlying mechanism of inactivation. The findings represent a major advance beyond the impactful first hERG cryo-EM study by MacKinnon and colleagues, which described the overall architecture of the open channel in which the voltage sensor domain and the pore are "nonswapped." That study also described lateral pockets that may help capture the many blockers to which hERG channels are famously susceptible. However, despite some efforts, the mechanism of inactivation was not well resolved. This is where the current study steps in.

The first of two key observations emerging from this study defines a novel pore structure for the inactivated state. The cryo-EM structures at high K confirm the canonical columnar structure of the conducting pore, whereas at low K, a condition that promotes inactivation, one of the selectivity filter residues (V625) is rotated. Its carbonyl oxygen, which in the high-K (open) conformation coordinates a permeating K ion, is rotated and its backbone amide instead faces the pore. As a consequence, the pore dilates at V625 and constricts at the level of S624 and G626. The path is no longer permeant. MD simulations comparing high- and low-K structures and trapping each conformation confirm that the channel conducts when the V625 carbonyl oxygen lines the pore and fails to conduct when it rotates away.

A revelation of H bonding networks beautifully illuminates previous functional studies and provides the second major observation of this study. S620, "behind" the pore residues and long known to be crucial for inactivation, is observed changing partners in high vs. low K. In the high-K (open) structure, the S620 hydroxyl sidechain interacts with the backbone amides of selectivity filter residues F627 and G626 to stabilize the columnar structure of the conducting pore. In the low-K (inactivated) structure, the S620 sidechain now interacts with the flipped V625 carbonyl oxygen, and the pore is dilated at that position and constricted at two others. The inability of mutant S620T to form this critical H bond behind the pore explains the functional S620T mutant phenotype, a stable open channel that does not inactivate within the physiological voltage range. Thus a long-standing question in the field has been resolved.

Fascinating new biology emerges with MD simulations addressing how changes in K channel occupancy within the pore influence its structure. In the low-K cryo-EM structure, it is apparent that the carbonyl oxygens at F627 and G628 at the most external sites of the selectivity filter are not optimally positioned; MD simulations show a correspondingly low energy barrier to K ion escape. Thus, the authors argue (and based on previous experimental evidence), evacuation of K from the pore is facilitated and entry to the inactivated state is initiated. Moreover, a remarkable propensity for the rotation of the V625 carbonyl oxygens out of the permeant pathway (at least one flips out 85% of the time) further reduces energy barriers to inactivation. Free energy measurements of the underlying rotation of the V625-G626 peptide linkage using umbrella sampling simulations support this explanation for the characteristic rapidity with which hERG channels inactivate. These are all really new and surprising observations contributing to a major advance in understanding inactivation in hERG.

The study also carries out a detailed comparison with the KcsA and, to a lesser extent Shaker. Over the years inactivation has been alternately imagined as a collapse of the outer mouth of the pore, or a dilation disrupting ion coordination, but this study provides a holistic picture in which inactivation arises from the position and mobility of selectivity filter residues coordinating permeation, their

interactions with surrounding partners, and the structural impact of the permeating ions themselves. This study shows how altering these parameters creates unique ways in which different channels inactivate.

Comments:

1. I do not think this was mentioned, but do the authors want to speculate on why mutations in F627 or G625 enhance inactivation? It seems reasonable based on data and modeling provided that these mutations would exacerbate the already weak coordination of K ions at the outer mouth of the pore, thus facilitating the exit of ions. In general I was wanting more discussion of known inactivation mutant phenotypes.
2. Although it is obliquely mentioned in the last sentence of the Discussion, I was missing any consideration of the inherent voltage sensitivity of inactivation. It is beyond the scope of the current study, but it is nonetheless the other major and unique aspect of hERG inactivation (in addition to speed) and deserves a bit of discussion.

Minor:

P. 6, Line 7: Define "soft knock-on."

P. 3, Line 33: Redundancy could be reduced in the phrase "the selectivity filter phenylalanine in the selectivity filter."

Fig. 1D, left panel. Interpreting this figure would be aided by other landmark labels – perhaps a shadow of the pore helix, and an indicator of the central axis.

Fig. 2E. The y axis should be specified either on the figure or in the legend.

Reviewer #3 (Remarks to the Author):

My expertise lies in Cryo-EM single particle analysis (SPA), and I will primarily focus on the Cryo-EM aspect. Human ether-a-go-go related gene (HERG) potassium channels exhibit uniquely rapid inactivation kinetics among K<sup>+</sup> channels. Using Cryo-EM, the authors determined the conductive and non-conductive selectivity filter structures of HERG in the presence of different K<sup>+</sup> concentrations. The structural analysis indicated that a flipping of the selectivity filter valine carbonyl oxygens between two conductive states. To validate this, an extensive analysis based on molecular dynamics (MD) simulations was conducted. The analysis highlighted a low energy barrier, leading to rapid kinetics, for the flipping of the valine 625 carbonyl oxygens. The flipping is facilitated by a previously unrecognized interaction between S620 and Y616, which stabilized the transition state between conducting and non-conducting structures. Furthermore, electrophysiology studies for activation assessments demonstrated that mutations to the residues involved in these interactions affected inactivation gating in HERG. Building upon these results, the authors proposed that inactivation is the result of a high propensity for the flipping of the selectivity filter valine carbonyl oxygens. However, the proposal heavily relies on the MD simulation studies, which, in turn, are contingent upon the qualities of models built from the Cryo-EM maps. As stated in the manuscript, the precise location of backbone carbonyl oxygens is difficult to determine at the resolutions of their Cryo-EM maps, and I concur with the authors on this point. Nevertheless, the subsequent validations are well-designed and persuasive. I believe that this approach has the potential to inspire other researchers grappling with similar challenges arising from insufficient resolution of their Cryo-EM maps. Therefore, it is crucial for the authors to address the following major points related to the quality of Cryo-EM maps.

Major Points:

[Major Point #1] To improve the local resolution of the selectivity filter area in the Cryo-EM maps, I suggest the authors consider conducting focused refinement using a 3D reference mask. This

refinement should specifically target the pore domain (PD), focusing on the region where local resolutions are highest (dark blue part) in Fig 1B, right panel. Alternatively, a mask including only the voltage sensor domain (VSD) and the pore domain (PD) may work as well. For this, I recommend excluding the detergent area.

[Major Point #2] The authors should provide an explanation for the large differences in resolutions (exceeding 0.1 Å) observed between (a) the half-maps FSC resolution at the 0.143 FSC criterion and (b) the map-to-model FSC resolution at the 0.5 FSC criterion. Theoretically, these two resolution values should be very close to each other, with (b) potentially being slightly lower than (a), empirically differing by at most ~0.1 Å. Therefore, Supplementary Fig 1 raises concerns about the possibility of over-fitting in the Cryo-EM maps (associated with (i), (ii), and (iii)). A potential explanation could be the use of different 3D reference masks for the calculation of (a) and (b). Additionally, the term "Gold-standard Fourier shell correlation (FSC) curve between the map and model" is not an appropriate term. "Gold-standard" indicates that a FSC curve is calculated using two maps from completely independent refinements (typically called "half maps"). Thus, please remove "Gold-standard" from the above sentence. Furthermore, the repetition of "Fourier shell correlation (FSC)" in this figure legend of Supplementary Fig 1 should be removed.

[Major Point #3] Please use DAQ Score (<https://em.kiharalab.org/algorithm/daqscore>), Q-scores (supported by PyMOL and UCSF Chimera), or a similar model fitting evaluation tool. This will serve as additional validation of the modeling qualities.

[Major Point #4] Because the main text lacks clarity regarding the maps (C1 or C4 map) used for model building, difference map calculation, and MD simulation, please add a flow chart in the manuscript (like Supplementary Fig S1A), explicitly indicating the use of C1, C4 maps, and PDBs for each step in these procedures.

[Major Point #5] Several statements contribute to confusion. In lines 12-15 on page 4, it is mentioned that "we solved the structures using C4 symmetry to improve the overall resolution (Fig 1A)." However, asymmetry is presumed in the subsequent analysis following Cryo-EM map reconstruction. Lines 2-3 on page 8 state that "There are differences in the density along the ion conduction pathway between the high-K and low-K structures when determined with C1 symmetry (Fig 3A)." The Figure Legend of Fig 3A on page 9 states that "Structures of high-K (left) and low-K (right) selectivity filters determined with C1 symmetry." From these statements, my understanding is that (1) there is no difference between C4 maps of high-K and low-K, (2) the C4 models (PDB 8U67 and 8U68) were not utilized for subsequent analyses and (3) the C1 models (PDB 8V7M and 8V7N) were employed for the MD simulations (i.e., the analyses based on 3.5 Å and 3.4 Å resolution maps). If so, to enhance clarity, please consider moving figures related to the C4 reconstructions to "Supplementary Material" and using the C1 results in the main text and figures. Alternatively, removing the C4 maps and models from the manuscript might help readers focus on the key points the authors intend to convey in this study.

[Major Point #6] Related to [Major Point #5], the following statements create a misleading impression regarding the relationship between the Cryo-EM work assuming C4 symmetry and MD simulations assuming asymmetry: (1) the figure legend of Fig 1B on page 5 states that "local resolution of cryo-EM maps solved using C4 symmetry," (2) lines 12-15 on page 4 state that "... the resolution in the selectivity filter region reaching 3.1 Å (high-K) and 2.9 Å (low-K) respectively (Fig 1B)." If the C1 models (PDB 8V7M and 8V7N) were employed for the MD simulations analyses, please provide the local resolution maps of C1 reconstructions, because these statements contribute an impression that MD simulation analyses are based on these local resolution values in my opinion. Additionally, please specify the algorithm used for the local resolution calculation. As many local resolution algorithms have no direct relationship with the gold standard FSC resolution, and values of local resolution are heavily dependent on each algorithm and input parameter settings, it is crucial to regard local resolution as a relative measure of resolution variations between different areas (e.g., local resolution

of an area is higher than one of another area).

[Major Point #7] Please provide the following final data of Cryo-EM SPA and PDB for all four structures in Supplemental Table S1:

- Final 3D Refinement Jobs: Full Map, Two Unfiltered Maps, 3D Angular Distribution (.bild), Input Reference Mask Map.
- Post Processing Jobs: Post-Processed Map (No-Masked), Input Reference Mask Map (one focused on the transmembrane section if applicable).

[Major Point #8] I recommend that the authors seek assistance from a professional editor for scientific writing, as there is a concerning number of careless mistakes. Examples are outlined as minor points (not an exhaustive list).

#### Minor Points In The Main Text And Figures:

[Minor Point 1] In line 33 on page 4, there is no "blue arrowhead in Fig 1D". Maybe "black arrowhead"?

[Minor Point 2] In the figure legend of Fig.1 (page 5), a closing parenthesis is missing in "cyclic nucleotide binding homology domain (cNBHD,".

[Minor Point 3] Please add side chain labels mentioned in the figure legend to Fig. 2C (page 7).

[Minor Point 4] In the figure legend of Fig. 2D (page 7), "NB different voltage range of protocols for S620T channels" is not a complete sentence.

[Minor Point 5] In line 23 on page 6, "black dashed lines in Fig 2B" does not match with the content. Maybe "green dashed lines"?

[Minor Point 6] In line 34 on page 6, please define what "SF" stands for.

[Minor Point 7] In lines 13-14 on page 13, please clarify which panel of Fig 3 is related to the following statement: "..., our structures show an interaction between N629 and Y616 that is preserved in both the high and low-K structures (Fig 3)".

[Minor Point 8] In the figure legend of Fig. 7 (page 14), the panel labels (B) and (C) are missing. The explanations of left (blue) and right (orange) are missing.

[Minor Point 9] In lines 43-44 on page 18, please provide "a soft mask including only the transmembrane domains" since it can influence on the reported resolution significantly.

[Minor Point 10] In lines 41-42 on page 21, is "five" in "Five different "clusters", with 0, 1, 2, 3 and 4 carbonyl oxygens pointing in" correct? Maybe "four clusters"?

#### Minor Points In "Supplementary Material":

[Minor Point 11] On page 2, "Supplementary Table S1" is missing from the table title.

[Minor Point 12] On page 2, please use "1.05" (instead of "1.1") in "Pixel size (Å)" as in the main text. Reporting the exact value of pixel size used in Cryo-EM data processing is important for reproducibility.

[Minor Point 13] On page 2, the values of "Initial particle images (no.)" are missing.

[Minor Point 14] On page 6, there is no explanation of asterisk "\*" in Supplementary Fig 3.

[Minor Point 15] On page 6, please explain what the authors are intended to show with "Isoleucine and valine" and "Glycine" plots in Supplementary Fig 3B and 3D.

[Minor Point 16] On page 12, the y-axis labels of right graphs in Supplementary Fig 8D are not fully visible.

[Minor Point 17] On page 13, what is "e" of "(e; yellow)" in the figure legend of Supplementary Fig 8C-D?

[Minor Point 18] On page 14, what is "a" of "(a; second column)" in the figure legend of Supplementary Fig 9A?

[Minor Point 19] On page 15, "Figure 4D-G" in the figure legend of Supplementary Fig 10 must be "Figure 4C-F".

[Minor Point 20] On page 16, the panel labels in Supplementary Fig 11 are inconsistent with the figure legend. There are no panel "A" and "B".

[Minor Point 21] On page 16, please explain where is  $(z \text{ (Å)} = 0, r \text{ (Å)} = 0)$  in Supplementary Fig 11.

[Minor Point 22] On page 16, to be consistent, "Phe627" should be "F627" in the figure legend of Supplementary Fig 11.

[Minor Point 23] On page 16, please explain the insets of models in the figure legend of Supplementary Fig 12B-D.

[Minor Point 24] On page 18, "Figure 4D-G" must be "Figure 4C-F".

#### Reviewer #4 (Remarks to the Author):

The reason why C-type inactivation is orders of magnitude faster in hERG than in other K<sup>+</sup> channels is still an open question. Understanding which features of the hERG channel are responsible for its fast inactivation is an interesting biophysical problem with important practical implications due to the role of this channel in the repolarization of cardiac cells. In this study, the mechanisms of hERG inactivation are analyzed using cryo-EM, electrophysiological measurements, and Molecular Dynamics simulations. Several interesting results concerning atomic interactions that contribute to the stability of the selectivity filter are reported, and a model of inactivation is proposed. According to this model, the channel rapidly becomes non-conductive due to a change in the orientation of the carbonyl oxygen of residues V625. This movement of V625 is facilitated by the interaction between S620 and Y616.

I think that the study provides robust data about the role of S620 in the dynamics of the selectivity filter. I am less convinced about the hypothesis that the flipped structure of V625 with the carbonyl oxygen pointing to the pore loop might represent an inactivated state of the channel. If this were the case, the flipped structure should correspond to a local energy minimum, separated from the local energy minimum that corresponds to the conductive state. Instead, the data reported in the study seems to imply the opposite. The estimated energy barrier between the two orientations of V625 is 4-5 kcal/mol, which is lower than the highest energy barrier associated with ion movements across the selectivity filter. This energy barrier depends on the orientation of S620 (in the direction of the

selectivity filter or toward Y616), but again, there is no significant energy barrier preventing the movement of S620, and so this residue cannot act as a sort of switch for inactivation (as implied by Figure 6). In my opinion, all these data prove that flipping of V625 happens on a time scale similar to the time scale of ion conduction, so it is part of the (peculiar) dynamical features of the hERG selectivity filter but it does not represent a transition to an inactivated state. The simulations of conduction events only prove (with limits discussed below) that ion movements are less likely when the carbonyl oxygen of V625 is oriented to the pore loop, but if the flipping movement is as fast as ion conduction the two configurations of the selectivity filter differentiated by V625 flipping are actually both part of the ensemble of configurations accessible by a conductive channel, they do not represent respectively a conductive and an inactivated state.

Despite this different interpretation of the results, this is an interesting study that presents relevant data about the selectivity filter of the hERG channel. Therefore, I think that it should be accepted for publication after reconsidering part of the data interpretation on the base of the comments above.

In the following I include some more technical comments on the MD simulations:

- The simulations in high K<sup>+</sup> were initialized with 5 K<sup>+</sup> ions inside the selectivity filter. According to the data presented here and previous literature, the contemporary presence of 5 ions inside the selectivity filter seems unlikely. Indeed, in both simulations, the number of ions inside the channel rapidly drops to 1 or 2. The anomalous starting configuration adopted might have an impact on the number of conduction events observed.
- More importantly, if I understand correctly, the starting configuration was different for the simulations in low K<sup>+</sup>. This is not explicitly stated in the Methods, but looking at Figures 1 and S6, it seems that the simulations at low K<sup>+</sup> were initialized without ions in S1, S2 and S3. The absence of ions in these sites is going to cause a distortion in the structure of the selectivity filter that might justify the lack of conduction events. I think that the two sets of simulations (using restraints to preserve respectively the high/low K<sup>+</sup> structures) should be initialized in the same way. Otherwise, it is hard to know if the difference in conductance is due to the alternative restraints adopted or to the different initial configurations.
- The set of initial ion configurations used to explore the effect of K<sup>+</sup> ions on the structure of the selectivity filter misses important configurations with ions in adjacent binding sites. Configurations with ions in S3 and S2 were observed to be the most stable ones in several potassium channels, including hERG [J Chem Inf Model. 2023 Jan 9;63(1):251-258], in simulations with both AMBER and CHARMM force fields [J Am Chem Soc. 2021 Aug 11;143(31):12181-12193][J Chem Theory Comput. 2023 May 9;19(9):2574-2589]. I think that these ion configurations should be included in the set, also considering that the contemporary presence of ions in S2 and S3 is likely to impact on the flipping properties of V625.
- In previous MD simulations of hERG with the CHARMM force field [Proc Natl Acad Sci. 2020 Feb 11;117(6):2795-2804][Sci Adv. 2021 Jan 29;7(5):eabd6203] the selectivity filter closes in a few hundreds of nanoseconds. Closure of the selectivity filter in this time scale is a known characteristic of the CHARMM force field [J Chem Theory Comput. 2020 Nov 10;16(11):7148-7159]. Closure events do not seem to take place in the solute tempering simulations presented here; otherwise, I would expect a completely different free energy profile for the permeating ions. It would be interesting to include a comment about this difference with previous literature in the manuscript.

We would like to thank the reviewers for their thorough and insightful comments. Our response to each comment is shown in blue text and where we have modified text in the manuscript in response to a reviewer's comment we have reproduced those changes in red text.

The most substantial change to the manuscript is that we have reanalysed the replica exchange data making use of trajectories for all replicas (using Multistate Bennett Acceptance Ratio, MBAR, Shirts et al., 2008) which has enabled us to quantify the impact of rotation of multiple V625 backbone carbonyl groups on K<sup>+</sup> occupancy in the filter (see new Figure 3D revealing the elimination of ion binding in central selectivity filter sites due to increased number of carbonyl flips). The new MBAR analysis of the REST2 simulations has also enabled us to improve our estimates of the free energy barriers for the transition between S620 sidechain interactions with the F627/G626 amide backbones and Y616 carbonyl backbone, when the V625 carbonyl is pointing inwards, and for the transition between S620 sidechain interactions with the Y616 carbonyl backbone and the V625 carbonyl backbone when the V625 backbone carbonyl is flipped to point away from the central axis (new Figure 4C-F). The rationale for these new analyses are detailed in the responses to Reviewer 4. The new analysis does not change the message of the paper, but rather reinforces the central hypothesis that a flipped V625 backbone carbonyl, when stabilized by interaction with the S620 sidechain, forms a non-conducting selectivity filter structure in HERG. We thank reviewer 4 for encouraging us to undertake this additional work.

#### Reviewer 1

The authors investigate a novel mechanism for HERG inactivation at the selectivity filter (C-type) by combining a novel HERG structure in very low K with MD simulation and mutagenesis analyses. In contrast to prior publications (Wang 2017 Cell, Li 2021 Sci Adv, Bassetto 2023 Nat Comm) that focus on a constriction between S1 and S2 caused by rearrangement of the uniquely displaced F627 residue, the evidence from the low K structure here points to the flipping of the V625 carbonyl oxygen out of the conduction path, leading to imperilled K transport due to a constriction between S3 and S4. Overall, the methods and data presented appear to be robust, and consistent with a novel mechanism activated in the low-K conditions. My concerns for this putative mechanism are that (1) it is derived primarily from simulations, whereas some prior experimental evidence suggests that it may be incorrect or need better explanation (see point 1 below), and (2) it is derived from the low-K condition, which may overlap voltage-dependent C-type inactivation but may point to a separate mechanism. Therefore, though I think this mechanism is plausible, the evidence presented here suggests that it may contribute to low-K inactivation rather than the primary driver of voltage-dependent HERG C-type inactivation.

The reviewer makes an important point about distinguishing between potassium dependence and voltage dependence of inactivation. It is for this reason that in the text of the original manuscript (and title) we were careful not to state that we have solved a structure of the inactivated state but rather that we had identified a non-conducting state. In contrast to the reviewer, we are inclined to hypothesise that the structure we have solved is of relevance to the inactivation observed under physiological voltages. Our reasons for making this suggestion are two-fold. First, comparing our two structures enables us to explain the importance of many of the residues that have been implicated, from mutagenesis studies, in inactivation (e.g. S620, F627, V625, N629, Q592). Although there are some residues that our structures do not provide insights into how they contribute to inactivation (e.g. N588). So we do not have the whole story. Second, in other K<sup>+</sup> channels, comparison of lowK and highK structures has largely replicated the conducting and non-conducting structures observed with mutants

that affect inactivation. We cannot say whether our hypothesis or that of the reviewer is correct but we feel our hypothesis is plausible and one that needs to be verified with further structural studies.

In response to these points we have expanded the discussion of the limitations of our proposed model: (see page 16, line 14-page 17, line 17)

Finally, there are some features of HERG inactivation that our model does not yet answer. For example, in the proposed three step mechanism, exit of ions from the extracellular filter, flipping of the V625 backbone carbonyls and stabilisation of the flipped V625 backbone carbonyl via its interaction with the S620 sidechain (Figure 6), we cannot determine which of these is the rate determining step. The free energy barrier for rotation of individual V625 backbone carbonyls is only 4-5 kcal/mol (Figure 3C) but from the REST2 simulations we suggest that at least 3 of the V625 backbone carbonyls will have to flip for the channel to become non-conducting. Furthermore, when a V625 backbone carbonyl initially flips, the S620 sidechain will be interacting with the Y616 backbone carbonyl and so the V625 backbone carbonyl is more likely to flip back (~1.8 kcal/mol free energy barrier) than remain flipped by interacting with the S620 sidechain (~6 kcal/mol free energy barrier). So, we suggest that flipping per se is not the rate limiting step. We cannot yet determine, however, whether the stabilisation of the flipped V625 backbone carbonyl by interaction with S620 sidechain or exit of K<sup>+</sup> ions from the extracellular end of the filter represents the rate limiting step. Another important consideration is that the energetics of K<sup>+</sup> ion-protein interactions are force field-dependent and distribution of ion configurations and their effects on filter structure may differ in other models. Our proposed model also does not address the origin of the voltage-sensitivity of HERG inactivation. Our cryoEM datasets, did not show significant rearrangements in the voltage sensor domain between conducting and non-conducting states (Figure 1C), consistent with much previous literature showing that mutations to charged residues in the voltage sensor domain have minimal impact on hERG inactivation<sup>45</sup>. The lack of any changes in the orientation of the extracellular S5P domain, between conducting and non-conducting states, was more surprising, given that mutations in the S5P domain have a profound effect on the voltage-sensitivity of HERG inactivation<sup>46</sup>. The changes in the height of the selectivity filter in the S631A mutant channel compared to low-K HERG channels (Figure 5) could provide a clue to the origin of voltage sensitivity, as these changes could alter the local electric field strength. Investigation of the voltage-sensitivity of HERG inactivation could be facilitated by structural studies of mutant channels with altered voltage sensitivity and/or analysis of channels in lipid vesicles that can be studied in the presence and absence of a voltage gradient as has recently been undertaken for HEAG channels<sup>47</sup>.

1. The mechanism demonstrated here seems to me inconsistent with prior experimental evidence showing enhanced (negatively-shifted) voltage-dependent inactivation of the Y616F mutant (Supp Fig 2, Kopfer Plos ONE 2012). A key point of the putative V625 mechanism is that S620 switches from binding G626 to V625 during inactivation, stabilizing the inactive conformation. For this to happen, there is a transient period of S620-Y616 binding, to lower the free energy barrier for V625 flipping. Thus, mutating Y616 should prevent inactivation, which the authors point out is consistent with non-inactivating Y616L mutants in Bassetto 2023. However, Y616 is shown to be a critical part of the activation pathway in that paper, and a substantial mutation such as Y616L appears to alter activation profoundly as well. This suggests that the Y616L mutant is likely altering the SF structure more globally and the effects on inactivation may not be specific to any particular mechanism. In contrast, the Y616F mutant studied in Kopfer is much more conservative, better maintaining the hydrophobic interactions that drive activation, but abolishing the hydrogen bonding that appears to be critical for the mechanism proposed here. This mutant would also be expected to distinguish between the V625

mechanism proposed here and the F627-Y616-N629 inactivation mechanism proposed by Li 2021 Sci Adv. In that paper, Y616-N629 bonding stabilizes the open conformation, whereas Y616-S620 interaction drives inactivation in the mechanism proposed here. If my understanding is correct, one would expect Y161F to enhance inactivation if the Li mechanism prevails, whereas it should abolish inactivation if the V625 mechanism proposed here is more important. Critically, Y616F appears to significantly enhance, rather than abolish, inactivation, and thus appears to suggest the F627 rearrangements are the critical factor. The authors would need to repeat the Y616F electrophysiology experiments to show different results (perhaps using different K concentrations to find a condition of abolished inactivation), or provide a different explanation (or what I may be missing in my interpretation), to reconcile this seemingly fundamental inconsistency. Nevertheless, to me this appears to suggest that the mechanism proposed here is less important for canonical HERG inactivation.

The reviewer raises an important point, re the effect of the Y616L and Y616F mutations. The most important point to make about our model is that the S620-Y616 interaction (that stabilizes the transition state between open and inactivated states) is an interaction between the S620 side chain hydroxyl and the Y616 backbone carbonyl (as stated many times in the manuscript, see e.g. the heading of the results section on p11: “The transition state between flipped and non-flipped V625 carbonyl oxygens is facilitated by an interaction between the S620 sidechain and Y616 backbone carbonyl”). After careful rereading of the manuscript, however, we note that we did not specifically mention Y616 backbone at the end of the paragraph at the top of p11 when we mentioned Y616L and we suspect that this is where the confusion arose. As the S620-Y616 interaction involves the Y616 backbone carbonyl, it is not a given that mutations to the Y616 sidechain would necessarily affect the S620-Y616 interaction. Accordingly, to remove any potential for confusion we have removed the reference to Y616L in this section (see page 12, lines 9-15).

This section of the text now read as follows:

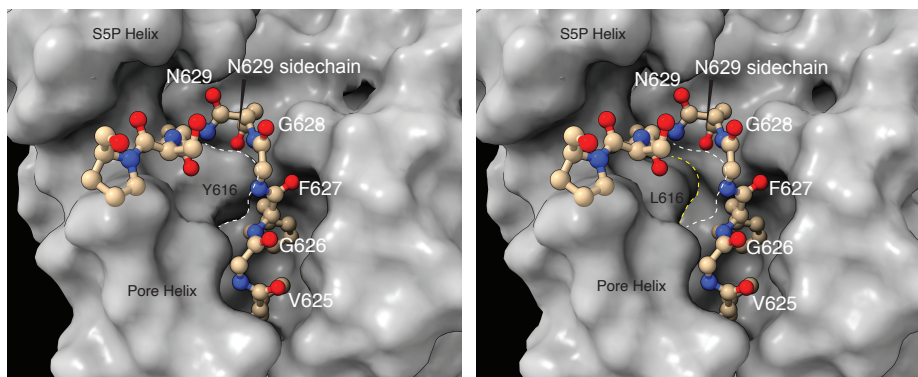
Thus, the S620 sidechain -Y616 backbone interaction acts like a catalyst to lower the free energy barrier of the transition state and enable rapid rotation of the V625 backbone carbonyl oxygen. When the V625 backbone carbonyl is flipped, the free energy barrier for S620 sidechain to switch between interacting with the Y616 backbone carbonyl oxygen and the V625 backbone carbonyl oxygen is  $5.9 \pm 0.5$  kcal/mol. We suggest that the V625 backbone carbonyl can rotate back and forth frequently but it needs to be trapped in the flipped state by an interaction with the S620 side chain to stabilize the non-conducting conformation.

The data about Y616L and Y616F is, however, more pertinent to understanding the interactions between the Y616 sidechain and the N629 sidechain, which our data show is present in both the conducting and non-conducting structures. Why Y616L and Y616F have different phenotypes is not straight forward but the reviewer has hinted at a plausible explanation. We agree that given Y616L alters activation profoundly as well, this suggests that the Y616L mutant may be altering the SF structure more globally and so cannot be easily interpreted. For the more conservative Y616F mutation, we suggest that it would affect the Y616-sidechain interaction with N629 in both states and so the overall effect would depend on whether that interaction was relatively more important (compared to other interactions) for stabilising the conducting or non-conducting states. If this interaction is more important for the open state then the open state would be perturbed more than the non-conducting state and the net effect would be to shift the equilibrium towards the inactivated

state. Accordingly, we have modified the discussion of the Y616-N629 interaction as follows (see page 15, lines 20-26):

Rather than interaction with S620, our structures show an interaction between the sidechains of N629 and Y616 that is preserved in both the high and low-K structures (Fig 2B) and so could serve to scaffold the upper part of the filter to the pore-helix in both conducting and non-conducting states. Given the tight packing in this area, it is perhaps not surprising that mutations to either N629 or Y616 either produce non-functional channels or have significant changes to function (e.g. N629D channels are non selective for K<sup>+</sup> over Na<sup>+</sup> <sup>44</sup> and Y616L alters both activation and inactivation <sup>39</sup>. Perhaps the most informative mutation is that of Y616F which removes a single hydroxyl sidechain. This mutation enhances inactivation which suggests that the interaction between the Y616 and N629 side chains is relatively more important for stabilising the open state than the inactivated state.

To fully explore this question however would necessitate determining structures of these mutations. Supporting this idea, introduction of Y616F or Y616L mutations into the HERG structure in Chimera, results in clashes which differ with each mutant. This strongly implies that the local structure will have to change to accommodate the mutations, and this will be slightly different for each mutant. To illustrate this problem, we have shown below images for a model of the Y616L mutant compared to WT. As can be seen the Leu sidechain occupies less volume in the region behind the upper part of the filter. This gap is unlikely to be filled with water, given the hydrophobic nature of the nearby sidechains so there will have to be some perturbation to the adjacent structural regions.



Left panel: CryoEM density for WT HERG with the Y616 sidechain highlighted by dashed line. The Selectivity filter and PS6 linker for the subunit corresponding to the highlighted Y616 is shown in ball and stick representation with backbone carbonyls labelled along with the N629 sidechain oxygen that interacts with Y616 hydroxyl. Right panel: computed cryoEM density for the Y616L mutation. The change in volume is indicated by the dashed lines. This “empty space” would not exist in a real structure but would require some adjustment to adjacent structures. How this occurs would be best addressed in cryoEM studies of mutant channels, which are beyond the scope of the present study.

Whilst we do not specifically mention these residues, we have modified the end of the discussion to make the more general point that determining how mutations in the vicinity of the SF affect inactivation will require new structural studies: (page 17, lines 19-23):

These subtle differences can explain the uniquely rapid inactivation kinetics of HERG channels and paves the way for future structural investigations into understanding how clinically occurring

mutations in the vicinity of the selectivity filter, as well as movement of the activation gate, alter the distribution between conducting and non-conducting states of HERG.

2. The structural work is intriguing in showing that the majority of rearrangement between high and low K structures to be centered on the selectivity filter. Given that they analyzed a large number of particles, Cryosparc 4.0 3D classification without alignment may resolve intermediate low-occupancy states that may help bolster the mechanism proposed.

Likewise, we had hoped to resolve substates which we tried to do using symmetry expansion in Relion. We were not able to see any differences amongst the eight classes, which may have been due to having insufficient resolution, insufficient number of particles and/or there are no intermediate states that are occupied for a sufficient period of time to enable them to be identified as a separate class. This, however, is consistent with the known rapidity of HERG inactivation, i.e. any intermediate states would be very transient.

We have added a sentence to the Cryo-EM data processing section of the methods to reflect this (see page 21, lines 42-45):

Focused refinement using a soft mask covering only the transmembrane region (398-667) was done using the final polished particles. Focused refinement did not improve resolution or provide better quality map and, therefore, the focused refined map was not used.

3. The electrophysiology data is poorly annotated. Methods say that both high and low K conditions were used, but this is not labelled nor described in the text. Y axis scale bars are missing.

The mention of low and high K conditions was a mistake and has now been corrected (see page 20, lines 27-28):

Perfusion solutions contained 3 mM KCl, 97 mM NaCl, 1.8 mM CaCl<sub>2</sub>, 1 mM MgCl<sub>2</sub>, 5 mM HEPES, pH adjusted to 7.5 with NaOH.

We did not include y-axis scale bars as current amplitude was not critical for interpretation of the data. We agree, however, that it is sensible to include this and have modified the figure and legend accordingly (see Figure 2D, page 8). We have also added labels for sidechains in Figure 2B as requested in point 4.

**D.** Exemplar families of current traces recorded from V625T and F627Y in WT and S620T backgrounds. Vertical scale bar is 500 nA in each panel.

4. For ease of understanding for a broader audience, it would be useful to label all the relevant figures (e.g. Fig. 1D, E, 2B, 3A, 4A, 6) with both S0-S4 as well as critical residues V625, F627, etc. This would make it much easier to understand which part of the selectivity filter is being diagrammed in each panel rather than having to jump back and forth between S0-S4 labelled panels and amino-acid labelled panels.

Thank-you for these suggestions which we have incorporated into the revised Figures 1 (page 6), 2 (page 8), 3 (page 11), 4 (page 12), 6 (page 14).

Reviewer 2

This manuscript by Lau et al. describes new insights into the rapid hERG inactivation process underlying this channel's key role in ventricular repolarization. Exploiting the K sensitivity characteristic of C-type inactivation to bias conformation toward the open or inactivated state, the authors used cryo-EM, electrophysiology, and molecular dynamics (MD) simulations to present a convincing picture of the underlying mechanism of inactivation. The findings represent a major advance beyond the impactful first hERG cryo-EM study by MacKinnon and colleagues, which described the overall architecture of the open channel in which the voltage sensor domain and the pore are "nonswapped." That study also described lateral pockets that may help capture the many blockers to which hERG channels are famously susceptible. However, despite some efforts, the mechanism of inactivation was not well resolved. This is where the current study steps in.

The first of two key observations emerging from this study defines a novel pore structure for the inactivated state. The cryo-EM structures at high K confirm the canonical columnar structure of the conducting pore, whereas at low K, a condition that promotes inactivation, one of the selectivity filter residues (V625) is rotated. Its carbonyl oxygen, which in the high-K (open) conformation coordinates a permeating K ion, is rotated and its backbone amide instead faces the pore. As a consequence, the pore dilates at V625 and constricts at the level of S624 and G626. The path is no longer permeant. MD simulations comparing high- and low-K structures and trapping each conformation confirm that the channel conducts when the V625 carbonyl oxygen lines the pore and fails to conduct when it rotates away.

A revelation of H bonding networks beautifully illuminates previous functional studies and provides the second major observation of this study. S620, "behind" the pore residues and long known to be crucial for inactivation, is observed changing partners in high vs. low K. In the high-K (open) structure, the S620 hydroxyl sidechain interacts with the backbone amides of selectivity filter residues F627 and G626 to stabilize the columnar structure of the conducting pore. In the low-K (inactivated) structure, the S620 sidechain now interacts with the flipped V625 carbonyl oxygen, and the pore is dilated at that position and constricted at two others. The inability of mutant S620T to form this critical H bond behind the pore explains the functional S620T mutant phenotype, a stable open channel that does not inactivate within the physiological voltage range. Thus a long-standing question in the field has been resolved.

Fascinating new biology emerges with MD simulations addressing how changes in K channel occupancy within the pore influence its structure. In the low-K cryo-EM structure, it is apparent that the carbonyl oxygens at F627 and G628 at the most external sites of the selectivity filter are not optimally positioned; MD simulations show a correspondingly low free energy barrier to K ion escape. Thus, the authors argue (and based on previous experimental evidence), evacuation of K from the pore is facilitated and entry to the inactivated state is initiated. Moreover, a remarkable propensity for the rotation of the V625 carbonyl oxygens out of the permeant pathway (at least one flips out 85% of the time) further reduces free energy barriers to inactivation. Free energy measurements of the underlying rotation of the V625-G626 peptide linkage using umbrella sampling simulations support this explanation for the characteristic rapidity with which hERG channels inactivate. These are all really new and surprising observations contributing to a major advance in understanding inactivation in hERG.

The study also carries out a detailed comparison with the KcsA and, to a lesser extent Shaker. Over the

years inactivation has been alternately imagined as a collapse of the outer mouth of the pore, or a dilation disrupting ion coordination, but this study provides a holistic picture in which inactivation arises from the position and mobility of selectivity filter residues coordinating permeation, their interactions with surrounding partners, and the structural impact of the permeating ions themselves. This study shows how altering these parameters creates unique ways in which different channels inactivate.

Comments:

1. I do not think this was mentioned, but do the authors want to speculate on why mutations in F627 or G625 enhance inactivation? It seems reasonable based on data and modeling provided that these mutations would exacerbate the already weak coordination of K ions at the outer mouth of the pore, thus facilitating the exit of ions. In general I was wanting more discussion of known inactivation mutant phenotypes.

Given that the critical interactions involve the backbone amides or carbonyls for F627, G626 and V625 it is difficult to predict what the effect sidechain mutations would have. We agree with the reviewer that it is plausible that mutations to F627 would exacerbate the already weak coordination of K ions at the outer mouth of the pore – however to comment on exactly how this occurs could only be speculation. Rather, we suggest that the only way to address this point directly would be to determine the structures of the mutant channels, which is beyond the scope of the present study. Nevertheless, we have modified the text at the end of the section “Different Hydrogen bond networks stabilize low-K and high-K structures of HERG” (page 7, lines 13-17) to address this point as follows:

It is not obvious how sidechain mutations to V625 and F627 affect inactivation as they will not directly affect the backbone carbonyls that are critical for co-ordinating K<sup>+</sup> ions. Given the tight packing in the local environment, it is plausible that conservative sidechain modifications are sufficient to alter the local environment but not to such a degree that it overcomes the effect of the S620T mutation to stabilize the conducting conformation.

The need for future structural investigations is also made at the end of our final discussion (page 17, lines 18-23):

In summary, the structure of the conducting filter for HERG resembles that seen for KcsA and Shaker, but the non-conducting filters are all different to each other. These subtle differences can explain the uniquely rapid inactivation kinetics of HERG channels and paves the way for future structural investigations into understanding how clinically occurring mutations in the vicinity of the selectivity filter, as well as movement of the activation gate, alter the distribution between conducting and non-conducting states of HERG.

2. Although it is obliquely mentioned in the last sentence of the Discussion, I was missing any consideration of the inherent voltage sensitivity of inactivation. It is beyond the scope of the current study, but it is nonetheless the other major and unique aspect of hERG inactivation (in addition to speed) and deserves a bit of discussion.

Thank-you for this suggestion. We have now added a section discussing this point (page 17, lines 5-17):

Our proposed model also does not address the origin of the voltage-sensitivity of HERG inactivation. Our cryoEM datasets, did not show significant rearrangements in the voltage sensor domain between conducting and non-conducting states (Figure 1C), consistent with much previous literature showing that mutations to charged residues in the voltage sensor domain

have minimal impact on hERG inactivation<sup>45</sup>. The lack of any changes in the orientation of the extracellular S5P domain, between conducting and non-conducting states, was more surprising, given that mutations in the S5P domain have a profound effect on the voltage-sensitivity of HERG inactivation<sup>46</sup>. The changes in the height of the selectivity filter in the S631A mutant channel compared to low-K HERG channels (Figure 5) could provide a clue to the origin of voltage sensitivity, as these changes could alter the local electric field strength. Investigation of the voltage-sensitivity of HERG inactivation could be facilitated by structural studies of mutant channels with altered voltage sensitivity and/or analysis of channels in lipid vesicles that can be studied in the presence and absence of a voltage gradient as has recently been undertaken for HEAG channels<sup>47</sup>.

Minor:

P. 6, Line 7: Define “soft knock-on.”

We have rephrased this sentence (see page 5, lines 16-18) to :

... showed a soft knock-on mechanism, i.e., there was a water molecule separating adjacent K<sup>+</sup> ions during the translocation of ions between S1-S2-S3-S4 K<sup>+</sup> ion binding sites.

P. 3, Line 33: Redundancy could be reduced in the phrase “the selectivity filter phenylalanine in the selectivity filter.”

The phrase has been modified to “the phenylalanine in the selectivity filter.” (page 3, line 33)

Fig. 1D, left panel. Interpreting this figure would be aided by other landmark labels – perhaps a shadow of the pore helix, and an indicator of the central axis.

We have modified Figure 1D by swapping the two images – and adding the location of ions S1-S4 to help orientate the viewer. We felt this was the simplest way to help orientate the viewer (see page 6)

Fig. 2E. The y axis should be specified either on the figure or in the legend.

A y-axis has now been specified in Figure 2E (page 8)

Reviewer 3

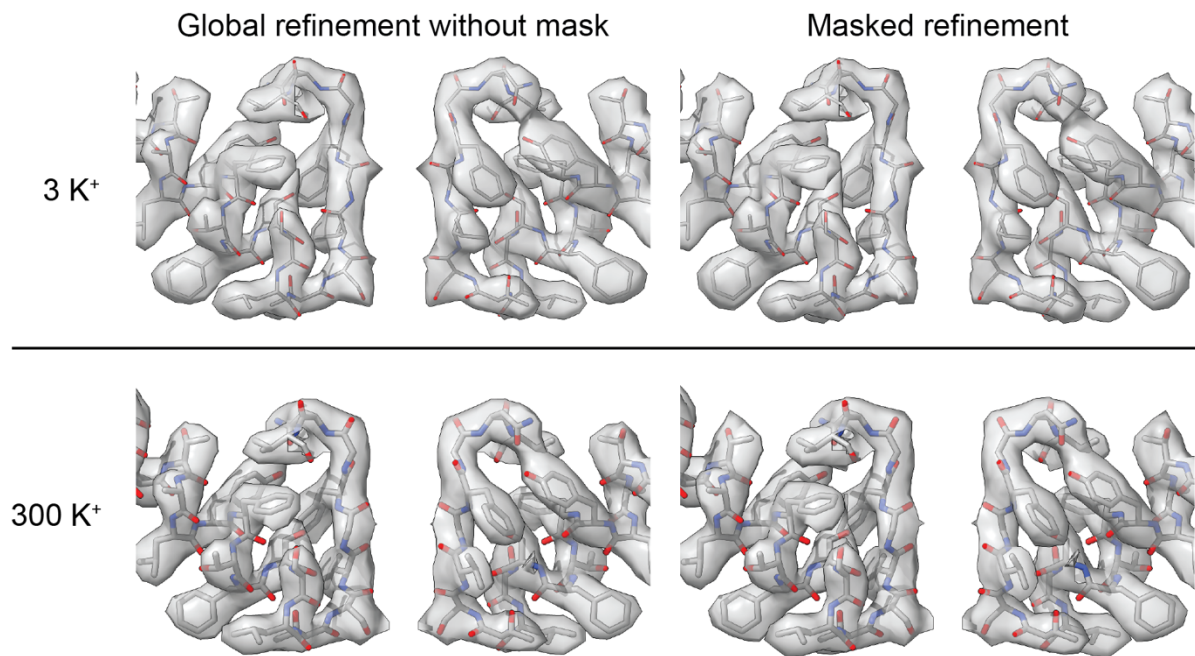
My expertise lies in Cryo-EM single particle analysis (SPA), and I will primarily focus on the Cryo-EM aspect. Human ether-a-go-go related gene (HERG) potassium channels exhibit uniquely rapid inactivation kinetics among K<sup>+</sup> channels. Using Cryo-EM, the authors determined the conductive and non-conductive selectivity filter structures of HERG in the presence of different K<sup>+</sup> concentrations. The structural analysis indicated that a flipping of the selectivity filter valine carbonyl oxygens between two conductive states. To validate this, an extensive analysis based on molecular dynamics (MD) simulations was conducted. The analysis highlighted a low free energy barrier, leading to rapid kinetics, for the flipping of the valine 625 carbonyl oxygens. The flipping is facilitated by a previously unrecognized interaction between S620 and Y616, which stabilized the transition state between conducting and non-conducting structures. Furthermore, electrophysiology studies for activation assessments demonstrated that mutations to the residues involved in these interactions affected inactivation gating in HERG. Building upon these results, the authors proposed that inactivation is the result of a high propensity for the flipping of the selectivity filter valine carbonyl oxygens. However, the proposal heavily relies on the MD simulation studies, which, in turn, are contingent upon the qualities of models built from the Cryo-EM maps. As stated in the manuscript, the precise location of backbone carbonyl oxygens is difficult to determine at the resolutions of their Cryo-EM maps, and I concur with the authors on this point. Nevertheless, the subsequent validations are well-designed and persuasive. I believe that this approach has the potential to inspire other researchers grappling with similar challenges arising from insufficient resolution of their Cryo-EM maps. Therefore, it is crucial for the authors to address the following major points related to the quality of Cryo-EM maps.

Major Points:

[Major Point #1] To improve the local resolution of the selectivity filter area in the Cryo-EM maps, I suggest the authors consider conducting focused refinement using a 3D reference mask. This refinement should specifically target the pore domain (PD), focusing on the region where local resolutions are highest (dark blue part) in Fig 1B, right panel. Alternatively, a mask including only the voltage sensor domain (VSD) and the pore domain (PD) may work as well. For this, I recommend excluding the detergent area.

We have performed focused refinement with mask including only the transmembrane/pore domain, the resulting map did not provide more information or resolution improvement. Below are comparisons of post-processed maps showing the selectivity filter area at 8  $\sigma$ . (see figure below). We have added also a sentence in the methods (page 21, lines 42-45) to highlight this point:

Focused refinement using a soft mask covering only the transmembrane region (398-667) was done using the final polished particles. Focused refinement did not improve resolution or provide better quality map and, therefore, the focused refined map was not used.



[Major Point #2] The authors should provide an explanation for the large differences in resolutions (exceeding 0.1 Å) observed between (a) the half-maps FSC resolution at the 0.143 FSC criterion and (b) the map-to-model FSC resolution at the 0.5 FSC criterion. Theoretically, these two resolution values should be very close to each other, with (b) potentially being slightly lower than (a), empirically differing by at most ~0.1 Å. Therefore, Supplementary Fig 1 raises concerns about the possibility of over-fitting in the Cryo-EM maps (associated with (i), (ii), and (iii)). A potential explanation could be the use of different 3D reference masks for the calculation of (a) and (b). Additionally, the term "Gold-standard Fourier shell correlation (FSC) curve between the map and model" is not an appropriate term. "Gold-standard" indicates that a FSC curve is calculated using two maps from completely independent refinements (typically called "half maps"). Thus, please remove "Gold-standard" from the above sentence. Furthermore, the repetition of "Fourier shell correlation (FSC)" in this figure legend of Supplementary Fig 1 should be removed.

Thank-you for pointing out this error. We used the wrong input model to calculate the model-map FSC curve. The final deposited PDB has now been used to recalculate the model-map FSC. Supplementary Table 1 and Supplementary Fig S1 (now supplementary Fig S2) have been updated with the correct model-map FSC resolution and the difference between half-map FSC and model-map FSC are now within 0.1 Å as suggested should be the case by the reviewer.

"Gold-standard" and the repeated "Fourier shell correlation (FSC)" has been removed from figure legend of Supplementary Fig 1 (now supplementary Fig S2). This part of the legend (see Supplementary material, page 5, lines 8-10) now reads as follows:

**F. Fourier shell correlation (FSC) curve between the map and model for (i) high-K with C4 symmetry, (ii) low-K with C4 symmetry, (iii) high-K with C1 symmetry, (iv) low-K with C1 symmetry.**

[Major Point #3] Please use DAQ Score (<https://em.kiharalab.org/algorithm/daqscore>), Q-scores (supported by PyMOL and UCSF Chimera), or a similar model fitting evaluation tool. This will serve as additional validation of the modeling qualities.

Thank-you for this suggestion. A Global Q-score for each model has been added to Supplementary Table 1 (see page 2 of supplementary material) and per residue Q-score mapped to coordinate model has been added to the new Supplementary Figure S2, panel D.

[Major Point #4] Because the main text lacks clarity regarding the maps (C1 or C4 map) used for model building, difference map calculation, and MD simulation, please add a flow chart in the manuscript (like Supplementary Fig S1A), explicitly indicating the use of C1, C4 maps, and PDBs for each step in these procedures.

A more detailed flow chart has been added (new Supplementary Fig S1). We have also altered the first paragraph of the results to make it clearer that all subsequent analyses (including templates for MD simulations) were based on C4 maps (page 4, lines 10-16):

To interrogate the potassium dependence of hERG channels we purified a WT hERG construct, with the predicted unstructured regions spanning residues 140-380 and 870-1006 deleted<sup>22</sup>, in buffers containing either 300mM KCl (high-K) or 3mM KCl (low-K). Structures were solved using relion; a flow chart summarising the EM data processing is shown in Supplementary Fig S1. Structures were initially solved with C1 symmetry, however, as there was no substantial asymmetry between subunits (Supplementary Fig S2), we solved the structures using C4 symmetry to improve the overall resolution (Fig 1A) and the C4 maps were used for all subsequent analyses.

We have also replaced the C1 maps in Figure 3A with C4 maps. A direct comparison of the C1 and C4 maps for the selectivity filter region are included in the new supplementary Figure S2, panel G.

[Major Point #5] Several statements contribute to confusion. In lines 12-15 on page 4, it is mentioned that "we solved the structures using C4 symmetry to improve the overall resolution (Fig 1A)." However, asymmetry is presumed in the subsequent analysis following Cryo-EM map reconstruction. Lines 2-3 on page 8 state that "There are differences in the density along the ion conduction pathway between the high-K and low-K structures when determined with C1 symmetry (Fig 3A)." The Figure Legend of Fig 3A on page 9 states that "Structures of high-K (left) and low-K (right) selectivity filters determined with C1 symmetry." From these statements, my understanding is that (1) there is no difference between C4 maps of high-K and low-K, (2) the C4 models (PDB 8U67 and 8U68) were not utilized for subsequent analyses and (3) the C1 models (PDB 8V7M and 8V7N) were employed for the MD simulations (i.e., the analyses based on 3.5 Å and 3.4 Å resolution maps). If so, to enhance clarity, please consider moving figures related to the C4 reconstructions to "Supplementary Material" and using the C1 results in the main text and figures. Alternatively, removing the C4 maps and models from the manuscript might help readers focus on the key points the authors intend to convey in this study.

Our intention with showing the C1 map was to minimize the potential for symmetry artefacts to obscure the densities along the central axis. We now compare both C1 and C4 maps in the new Supplementary Figure 2G, but to remove any potential for confusion with regards the subsequent MD studies, we show the C4 maps in the new Figure 3. The starting template for the MD simulations was the C4 maps. However, as all atoms in the simulations are allowed to vary independently at any one point in time there are always subtle differences between each subunit, hence the reason the subunits were analysed independently in the MD simulations.

[Major Point #6] Related to [Major Point #5], the following statements create a misleading impression regarding the relationship between the Cryo-EM work assuming C4 symmetry and MD simulations assuming asymmetry: (1) the figure legend of Fig 1B on page 5 states that "local resolution of cryo-EM maps solved using C4 symmetry," (2) lines 12-15 on page 4 state that "... the resolution in the selectivity filter region reaching 3.1 Å (high-K) and 2.9 Å (low-K) respectively (Fig 1B)." If the C1 models (PDB 8V7M and 8V7N) were employed for the MD simulations analyses, please provide the local resolution maps of C1 reconstructions, because these statements contribute an impression that MD simulation analyses are based on these local resolution values in my opinion. Additionally, please specify the algorithm used for the local resolution calculation. As many local resolution algorithms have no direct relationship with the gold standard FSC resolution, and values of local resolution are heavily dependent on each algorithm and input parameter settings, it is crucial to regard local resolution as a relative measure of resolution variations between different areas (e.g., local resolution of an area is higher than one of another area).

With respect to the determination of local resolution, this was calculated using RELION's implementation of local resolution estimation. This has been added to the Methods section (see page 21, lines 46-48).

Post-processing and resolution estimates were performed with a soft mask including only the transmembrane domains. Local resolution was calculated using the local resolution function in Post-processing job of Relion.

We agree with the reviewer's concern that the calculation of local resolution is inexact but that relative differences are still valid. Accordingly, we have left the local resolution maps in Figure 1B which clearly illustrate that the local resolution is highest in the vicinity of the selectivity filter and modified the main text (see page 4, lines 16-19):

The global resolution was 3.3 Å for high-K<sup>+</sup> and 3.0 Å for low-K<sup>+</sup> (Fig 1B, Supplementary Fig S1, Supplementary Table S1). The local resolution was highest in the vicinity of the selectivity filter region in both the highK and lowK structures ( Fig 1B).

As per major point 5 we have removed C1 maps from Figure 3 to make it clear that the templates for the MD simulations were based on the C4 maps. Whilst the MD simulations start with C4 maps – as each atom (and therefore each subunit) is allowed to fluctuate independently it is not surprising that there are asymmetries in the atomic level fluctuations.

[Major Point #7] Please provide the following final data of Cryo-EM SPA and PDB for all four structures in Supplemental Table S1:

- Final 3D Refinement Jobs: Full Map, Two Unfiltered Maps, 3D Angular Distribution (.bild), Input Reference Mask Map.

- Post Processing Jobs: Post-Processed Map (No-Masked), Input Reference Mask Map (one focused on the transmembrane section if applicable).

All these files will be publicly available when the structures are released on the pdb and EMDB. In the meantime, we have uploaded the files to the Nature Comms portal for reviewers to access.

[Major Point #8] I recommend that the authors seek assistance from a professional editor for scientific writing, as there is a concerning number of careless mistakes. Examples are outlined as minor points

(not an exhaustive list).

#### Minor Points In The Main Text And Figures:

[Minor Point 1] In line 33 on page 4, there is no “blue arrowhead in Fig 1D”. Maybe “black arrowhead”?

“blue” has been deleted from legend for Figure 1D (page 6)

[Minor Point 2] In the figure legend of Fig.1 (page 5), a closing parenthesis is missing in “cyclic nucleotide binding homology domain (cNBHD,”.

Closing bracket has been added (page 6)

[Minor Point 3] Please add side chain labels mentioned in the figure legend to Fig. 2C (page 7).

Sidechain labels have been added to Figure 2C (see page 8)

[Minor Point 4] In the figure legend of Fig. 2D (page 7), “NB different voltage range of protocols for S620T channels” is not a complete sentence.

This has been modified as follows:

Note the different range of voltages used for tail current recordings for S620T channels. (page 8)

[Minor Point 5] In line 23 on page 6, “black dashed lines in Fig 2B” does not match with the content. Maybe “green dashed lines”?

The legend for Figure 2B has been changed to “green dashed lines” (see page 8)

[Minor Point 6] In line 34 on page 6, please define what “SF” stands for.

This has been changed to “selectivity filter” (see page 6, figure legend 1E)

[Minor Point 7] In lines 13-14 on page 13, please clarify which panel of Fig 3 is related to the following statement: “..., our structures show an interaction between N629 and Y616 that is preserved in both the high and low-K structures (Fig 3)“.

This has been corrected to “Fig 2B” (page 15, line 19)

[Minor Point 8] In the figure legend of Fig. 7 (page 14), the panel labels (B) and (C) are missing. The explanations of left (blue) and right (orange) are missing. ✓

The figure legend has been amended (see page 16):

Structures of the conducting (blue) and non-conducting (orange) filters for Shaker, KcsA, and

HERG. **A.** In Shaker channels there is dilatation of the central glycine and tyrosine carbonyl oxygens but little change in the lower filter<sup>18,19</sup>. **B.** In KcsA, the non-conductive state is

characterized by constriction of the central glycine carbonyl oxygens, an incomplete rotation of the valine carbonyl oxygens away from the central axis<sup>10</sup> and changes in water occupancy<sup>17</sup>. **C.**

The non-conductive state in HERG is more like KcsA than Shaker but involves a complete rotation of the V625 carbonyl oxygens, stabilized by an interaction with the S620 sidechain and no change in the number of water molecules.

[Minor Point 9] In lines 43-44 on page 18, please provide “a soft mask including only the transmembrane domains” since it can influence on the reported resolution significantly.

The mask has been uploaded with the other maps requested by reviewer and will be available through EMDB when published.

[Minor Point 10] In lines 41-42 on page 21, is “five” in “Five different “clusters”, with 0, 1, 2, 3 and 4 carbonyl oxygens pointing in” correct? Maybe “four clusters”?

The REST2 data have been reanalysed and so this section of text is no longer present. With the new analysis we are able to separate into all five cases of 0,1,2,3, or 4, flipped V625 backbone carbonyls, albeit there is insufficient data to fully capture the all four flipped case (see new Figure 3D, page 11).

Minor Points In “Supplementary Material”:

[Minor Point 11] On page 2, “Supplementary Table S1” is missing from the table title.  
“Supplementary Table S1” has been added.

[Minor Point 12] On page 2, please use “1.05” (instead of “1.1”) in “Pixel size (Å)” as in the main text. Reporting the exact value of pixel size used in Cryo-EM data processing is important for reproducibility.  
Pixel size has been changed to 1.05.

[Minor Point 13] On page 2, the values of “Initial particle images (no.)” are missing.  
Values of “Initial particle images (no.)” have been added.

[Minor Point 14] On page 6, there is no explanation of asterisk “\*” in Supplementary Fig 3.  
Explanation of asterisk has been added to the legend (new supplementary Figure 4, see page 7):  
Residues with Ramachandran probability in allowed but not favored region are marked with asterisk (\*).

[Minor Point 15] On page 6, please explain what the authors are intended to show with “Isoleucine and valine” and “Glycine” plots in Supplementary Fig 3B and 3D. ✓  
The following explanation has been added to the legend for the new Figure S4 (old Figure S3, see page 7):.

Ramachandran plots for V625, G626, and G628 are plotted separately based on different Ramachandran probability distribution of these residues.

[Minor Point 16] On page 12, the y-axis labels of right graphs in Supplementary Fig 8D are not fully visible.  
This is now supplementary Figure 9D and panel D has been removed as we have redone the REST2 analysis (see responses to Reviewer #4)

[Minor Point 17] On page 13, what is “e” of “(e; yellow)” in the figure legend of Supplementary Fig 8C-D?  
“(e, yellow)” is redundant as Yellow is referred to in the previous sentence. This part of the legend now reads as follows (page 15, lines 16-20):

When three V625 carbonyl oxygens were pointing in towards the channel axis (31% of the time; shown in yellow), there was an average of 1.9 ions in the selectivity filter maintaining good binding in all sites with the most common configurations being S3 alone, S1S3, and S2S4 (depicted in inset).

[Minor Point 18] On page 14, what is “a” of “(a; second column)” in the figure legend of Supplementary Fig 9A?  
This has been amended to (see columns 1,2 in panel A of the new Supplementary Fig S10, page 17)

[Minor Point 19] On page 15, “Figure 4D-G” in the figure legend of Supplementary Fig 10 must be “Figure 4C-F”.

“Figure 4D-G” has been changed to “Figure 4C-F” in the legend to the new Supplementary Figure S11 (page 18)

[Minor Point 20] On page 16, the panel labels in Supplementary Fig 11 are inconsistent with the figure legend. There are no panel “A” and “B”. ✓

Labels A,B,C are now included in the new supplementary Fig 12 (page 19)

[Minor Point 21] On page 16, please explain where is ( $z$  (Å) = 0,  $r$  (Å) = 0) in Supplementary Fig 11.

Although not specified especially for this figure, all analysis refers to positions relative to the centre of mass of the selectivity filter, as specified in the Methods section. To clarify in this case, the legend (new supplementary Fig S12) has been modified (see page 19) to include the following sentence:

$r = 0$  Å represents the central axis of the pore,  $z = 0$  Å represents the vertical component of the centre of mass of the selectivity filter.

[Minor Point 22] On page 16, to be consistent, “Phe627” should be “F627” in the figure legend of Supplementary Fig 11. ✓

“Phe627” has been changed to “F627” in the legend to the new supplementary Fig S12 (page 19):

There is also an increase in water bound to the F627 backbone amide when the V625 carbonyl oxygen is flipped, that compensates for F627 no longer interacting with S620.

[Minor Point 23] On page 16, please explain the insets of models in the figure legend of Supplementary Fig 12B-D.

We have modified the legend (now supplementary Figure S13) on page 20: to:

B-D. 2-dimensional free energy maps showing the pinching of G626 C $\alpha$  based on the distance between opposing subunits in: B) REST2 simulations, C ) MD simulations with ions constrained in S0/S2/S4; Di) MD simulations for an empty selectivity filter. Insets show representative cross section images at the level of G626 C $\alpha$ . Dii. 2-dimensional free energy map showing the relationship between the radial positions of G626 C $\alpha$  in two opposing subunits during the pinching of G626

[Minor Point 24] On page 18, “Figure 4D-G” must be “Figure 4C-F”. ✓

“Figure 4D-G” has been changed to “Figure 4C-F”.

## Reviewer #4 (Remarks to the Author):

The reason why C-type inactivation is orders of magnitude faster in hERG than in other K<sup>+</sup> channels is still an open question. Understanding which features of the hERG channel are responsible for its fast inactivation is an interesting biophysical problem with important practical implications due to the role of this channel in the repolarization of cardiac cells. In this study, the mechanisms of hERG inactivation are analyzed using cryo-EM, electrophysiological measurements, and Molecular Dynamics simulations. Several interesting results concerning atomic interactions that contribute to the stability of the selectivity filter are reported, and a model of inactivation is proposed. According to this model, the channel rapidly becomes non-conductive due to a change in the orientation of the carbonyl oxygen of residues V625. This movement of V625 is facilitated by the interaction between S620 and Y616.

I think that the study provides robust data about the role of S620 in the dynamics of the selectivity filter. I am less convinced about the hypothesis that the flipped structure of V625 with the carbonyl oxygen pointing to the pore loop might represent an inactivated state of the channel. If this were the case, the flipped structure should correspond to a local free energy minimum, separated from the local free energy minimum that corresponds to the conductive state. Instead, the data reported in the study seems to imply the opposite. The estimated free energy barrier between the two orientations of V625 is 4-5 kcal/mol, which is lower than the highest free energy barrier associated with ion movements across the selectivity filter.

This free energy barrier depends on the orientation of S620 (in the direction of the selectivity filter or toward Y616), but again, there is no significant free energy barrier preventing the movement of S620, and so this residue cannot act as a sort of switch for inactivation (as implied by Figure 6).

In my opinion, all these data prove that flipping of V625 happens on a time scale similar to the time scale of ion conduction, so it is part of the (peculiar) dynamical features of the hERG selectivity filter but it does not represent a transition to an inactivated state.

In the simulations shown in Figure 1F it is clear that when all four valine carbonyls are flipped that we do not see conduction. Nevertheless, the reviewer is right that the timescales for ion conduction (on the order of 50 ns, see e.g. Figure 1) and flipping of an individual valine carbonyl are comparable. From the analysis of the REST2 datasets provided in the original version of the manuscript we were not able to clarify for certain how different numbers of flipped valine carbonyls affected the free energy associated with the density of ions along the channel axis:  $\Delta G(z) = -k_B T \ln \rho(z) + C$ . To address this issue, we have reanalysed the REST2 data using MBAR (see updated methods section on page xxxx). This has enabled us to analyse information from all 16 replicas to obtain the best estimate of free energies within the unscaled replica. Because of the much greater sampling, this has permitted us to quantify the effect of 0, 1, 2, or 3 (and to some extent 4) flipped valine carbonyls on the free energy associated with the density of ions along the channel axis (new Figure 3D). This new analysis shows that there are ~4 kcal/mol free energy wells for ion occupancy in S1, S2, and S3, when there are no carbonyls flipped. These wells are destabilized by 0.5-1 kcal/mol with 1 or 2 valine carbonyls flipped but by 2-3 kcal/mol when three valine carbonyls are flipped, with similar observations for the partial sampling of 4 flipped carbonyls. Effectively, the flipping of 3-4 carbonyl groups leads to elimination of much of the ion binding in the central filter sites. We appreciate that this should be viewed as an indicator only as we have performed a simulation in the presence of high K<sup>+</sup>. However, it is consistent with the suggestion that there needs to be more than one valine carbonyl flipped to stop conduction. As such we cannot equate the free energy barrier for flipping of a single carbonyl (as shown in the old Figure 3D, new Figure 3C) to the free energy barrier for inactivation. Thus, it is

plausible that the rate for transition to an inactivated state may be considerably slower than that for transition for flipping of a single V625 carbonyl.

In addition to providing a new Figure 3D for the new REST2 analysis (page 11) we have made substantial changes to the text describing this figure (see page 10, lines 11-19)

We next analysed the free energy profile of ion distribution in the filter according to the number of flipped V625 backbone carbonyls (Fig 3D). Using Multistate Bennett Acceptance Ratio (MBAR)<sup>34</sup>, we exploit the sampling in all 16 REST2 replicas to obtain an optimal estimate of free energies in the unscaled replica. We achieve good sampling of wells and barriers for 0-3 flips, but only capture the low free energy regions with 4 flips. The free energy wells for S1, S2 and S3 are 3-4 kcal/mol deep when 0, 1, or 2 V625 backbone carbonyls are flipped, but become significantly destabilized when 3 or 4 V625 backbone carbonyls are flipped. This suggests that 0,1 or 2 flipped V625 backbone carbonyls are consistent with a conductive conformation whilst 3 or 4 flipped V625 backbone carbonyls may relate to the non-conducting form of the channel.

We have also modified the text in the discussion to reflect the observation that we likely need at least three V625 backbone carbonyls to flip to achieve a non-conducting state. Page 13: lines 23-25

The non-conducting state is stabilized by the flipped V625 backbone carbonyl binding to the S620 side chain and it is likely that at least three V625 backbone carbonyls need to flip for the channel to become non-conductive (Fig 3D).

To address the point re whether the flipped structure should correspond to a local free energy minimum, we also reanalysed the 2D PMF for S620 sidechain interactions with the V625 backbone carbonyl, G626/F627 backbone amides and the Y616 backbone carbonyl using the new Mbar analysis of the entire REST2 dataset. Qualitatively, the new analysis (new Figure 4C-F) is very similar to the old analysis (Figure 4C-F of previous manuscript) with four clear free energy minima corresponding to the S620 sidechain interacting with either (i) F627/G626 backbone amides or (ii) Y616 backbone carbonyl when the V625 carbonyl points towards the central axis and when the V625 carbonyl if flipped to point outwards the S620 sidechain can interact with (iii) Y616 backbone carbonyl or (iv) V625 backbone carbonyl. With the greatly improved sampling we can get quantitative estimates of the free energy barriers separating these four free energy minima. When the S620 sidechain is interacting with the Y616 backbone carbonyl, there is a  $1.8 \pm 0.1$  kcal free energy barrier for flipping of the V625 backbone carbonyl. Conversely, the barriers for transition from Y616 to G626/F627 interactions (V625 backbone carbonyl pointing inwards) or Y616 to V625 (V625 backbone carbonyl pointing outwards) are both of the order of 6 kcal/mol.

We have modified the text to reflect these changes (see page 11, line 11 – page 12, line 15):

To explore this hypothesis, we next analyzed 2D free energy surfaces for S620 sidechain interactions with selectivity filter residues and Y616 as a function of the angle of rotation of the V625 backbone carbonyl in the REST2 simulations with MBAR which allows more complete sampling of all states (Figure 4C-F). The four interactions that the S620 sidechain can participate in, occupy wells in the 2D free energy surfaces that are labelled (i) F627/G626 amides when the V625 backbone carbonyls point inwards, (ii) Y616 backbone carbonyl oxygen when the V625 backbone carbonyls point inwards (iii) Y616 backbone carbonyl when the V625 backbone carbonyls point outwards and (iv) V625 backbone carbonyl when the V625 backbone carbonyl point inwards in Fig 4C-F. When S620 is interacting with the Y616 backbone, the free energy barrier for valine flipping is only  $1.8 \pm 0.1$  kcal mol<sup>-1</sup>, whereas the transition is otherwise forbidden (Fig 4F). Thus, the S620 sidechain -Y616 backbone interaction acts like a catalyst to lower the free energy barrier of the transition state and enable rapid rotation of the V625 backbone carbonyl oxygen. When the V625 backbone carbonyl is flipped, the free energy barrier for S620 sidechain to switch between interacting with the Y616 backbone carbonyl oxygen and the V625 backbone carbonyl oxygen is  $5.9 \pm 0.5$  kcal/mol. Thus, we

suggest that the V625 backbone carbonyl can rotate back and forth frequently but occasionally will be trapped in the flipped state by an interaction with the S620 side chain, which likely represents the non-conducting conformation.

Based on the data presented in the new Figure 4C-F (plus the data from Figure 3D) rotation of a single V625 carbonyl can happen rapidly but is not sufficient to lead to a non-conducting state. Rather, the non-conducting state likely requires at least three flipped V625 carbonyls and the S620 sidechain needs to switch from interacting with the Y616 backbone carbonyl to bind to and stabilize the flipped V625 backbone carbonyl. A more extensive analysis of the impact of 1,2,3 & 4 flipped V625 carbonyls on conduction and stabilisation of the non-conductive state versus conductive states is beyond the scope of the present study but should be pursued in future studies.

In light of our new analyses, we have modified our proposed model of inactivation to include three steps: (i) exit of K<sup>+</sup> ions from the extracellular end of the filter (ii) flipping of the V625 backbone carbonyl when the S620 side chain is bound to Y616 and (iii) stabilisation of the flipped V625 backbone carbonyl by binding to the S620 sidechain. As the reviewer correctly points out, we still cannot definitively determine which is the rate limiting step in this model. It could be the exit of K<sup>+</sup> and altered conformation of the extracellular half of the filter, or the transition from S620 interaction with Y616 to V625 backbone carbonyl. To highlight this point we have made modifications to the discussion (see page 14, line 22 - page 15, line 10):

The interaction between the flipped V625 backbone carbonyls and the S620 sidechain hydroxyl in HERG likely contributes to stabilizing the “non-conducting” conformation of HERG. Thus, HERG may adopt two modes with V625 backbone carbonyls flipping back and forth (whilst the S620 sidechain is bound to the Y616 backbone carbonyl oxygen) and a longer-lived flipped state when the flipped V625 backbone carbonyl oxygen interacts with the S620 sidechain. Conversely, in KcsA rapid flipping of the V76 backbone carbonyls is associated with a flickering state<sup>41,42</sup> whereas in the inactivated state there is an increase in water behind the filter with the four V76 backbone carbonyls rotated ~90° away from the central axis where they form a ring-like water-mediated hydrogen bonding network that stabilizes the constricted structure<sup>16</sup>. A similar mechanism has also been observed in MthK channels<sup>30</sup>. It is not possible to observe water molecules at the resolution of our cryo-EM structures, but our MD simulations suggest that there is only a modest rearrangement with no net change in the number of water molecules behind the filter during the transition between conducting and non-conducting states (Supplementary Fig 12), albeit with the appearance of a free energy minimum that demonstrates a water molecule is driven down towards the flipped V625 upon change to the nonconducting state. The no net change in water molecules may also contribute to kinetics of HERG inactivation being faster than that observed for KcsA where the rate of inactivation is determined by the diffusion limited rate of water binding<sup>17</sup>.

And on page 16, line 14 - page 17, line 3:

Finally, there are some features of HERG inactivation that our model does not yet answer. For example, in the proposed three step mechanism, (i) exit of ions from the extracellular half of the filter, (ii) flipping of the V625 backbone carbonyls and (iii) stabilisation of the flipped V625 backbone carbonyl via its interaction with the S620 sidechain (Figure 6), we cannot determine which of these is the rate determining step. The free energy barrier for rotation of individual V625 backbone carbonyls is only 4-5 kcal/mol (Figure 3C) but from the REST2 simulations we suggest that at least 3 of the V625 backbone carbonyls will have to flip for the channel to become non-

conducting. Furthermore, when a V625 backbone carbonyl initially flips, the S620 sidechain will be interacting with the Y616 backbone carbonyl and so the V625 backbone carbonyl is more likely to flip back (~1.8 kcal/mol free energy barrier) than remain flipped by interacting with the S620 sidechain (~6 kcal/mol free energy barrier). So, we suggest that flipping *per se* is not the rate limiting step. We cannot yet determine, however, whether the stabilisation of the flipped V625 backbone carbonyl by interaction with S620 sidechain or exit of K<sup>+</sup> ions from the extracellular end of the filter represents the rate limiting step.

The simulations of conduction events only prove (with limits discussed below) that ion movements are less likely when the carbonyl oxygen of V625 is oriented to the pore loop, but if the flipping movement is as fast as ion conduction the two configurations of the selectivity filter differentiated by V625 flipping are actually both part of the ensemble of configurations accessible by a conductive channel, they do not represent respectively a conductive and an inactivated state.

Whilst we cannot put numbers on the conducting and flipping rates, we accept the argument of the reviewer that they are likely to be of similar order of magnitude and so individual V625 backbone carbonyl flipping may not be sufficient to reach a stable non-conducting state, but rather collective flipping of 3-4 V625 carbonyls may be needed and they need to be stabilised by the transition from S620 interacting with Y616 to S620 interacting with V625 backbone carbonyl. Whilst we can state that, when all four V625 carbonyls have flipped, the barrier to permeation is insurmountable and no conduction is observed (Figure 1F) the new analyses provided in the revised Figure 3D suggest that flipping of 1 or 2 V625 carbonyls may be permissive of ion conduction. Demonstration of this would require further investigation with simulations of conduction for 1,2,3 flipped V625 in future studies, but the evidence that ion binding is largely eliminated with 3-4 flips in Fig 3D suggests this likely outcome. This overlaps with that raised in the point above and is addressed in the limitations paragraph that has been added immediately before the conclusion (see above).

In the text of the original manuscript (and title) we were careful not to state that we have solved a structure of the inactivated state but rather that we had identified a non-conducting state. In the discussion we did, however, hypothesise that flipped V625 carbonyls, stabilized by interaction with S620 sidechain hydroxyl, could represent the inactivated state (most clearly in Figure 6). This model could be verified with further structural studies of mutant channels as mentioned at the end of the discussion. We do, however, agree with the reviewer that we have not determined the rate limiting step, which is also mentioned in the new limitations paragraph (see above)

Despite this different interpretation of the results, this is an interesting study that presents relevant data about the selectivity filter of the hERG channel. Therefore, I think that it should be accepted for publication after reconsidering part of the data interpretation on the base of the comments above.

In the following I include some more technical comments on the MD simulations:

1. - The simulations in high K<sup>+</sup> were initialized with 5 K<sup>+</sup> ions inside the selectivity filter. According to the data presented here and previous literature, the contemporary presence of 5 ions inside the selectivity filter seems unlikely. Indeed, in both simulations, the number of ions inside the channel

rapidly drops to 1 or 2. The anomalous starting configuration adopted might have an impact on the number of conduction events observed.

We included 5 ions in the selectivity filter (S0, S1, S2, S3 & S4; although S0 is external to the filter *per se*) initially to ensure that the filter was primed for conduction, even though this high free energy configuration is not expected to last beyond the initial equilibration stage. Our previous experience with other K channels has shown us that commencing with a water-intercalated ion configuration can lead to a period of hundreds of nanoseconds before knock-on conduction commences. As the sole purpose of these tests was to see if the pore is capable of supporting ion conduction, we deemed the five-ion configuration to be an appropriate initiation point. During the equilibration phase (panels now shown in the new supplementary Fig S7; panel G for the conducting case), it can be seen that the ions stay inside the filter while restrained in the first 10ns (with restraints slowly turned off; as described in the original Methods and now shown on page 23, lines 35-43) but then the outermost ions immediately leave (reducing occupancy to 3 ions) and then, after ~18ns, water molecules begin to insert between the ions, leading to 500ns of dynamics (Figure S7B) that is uncorrelated with the initial build. The lack of correlation to the initial build is evidenced by the distinct and random sampling of ion translocation events in the two replicated conduction simulations shown (Supplementary Fig S7B; panels (i) and (ii)). Moreover, we did not include the initial equilibration period in our analyses. This was stated in the methods for the constrained ion MD simulations but we did not repeat this statement in the description of the conduction MD methods, which we have now corrected (see page 25, lines 40-42):

During equilibration, heavy atom harmonic position restraints on the selectivity filter and resident ions were applied with a force constant of 5 kcal/mol/Å<sup>2</sup>, relaxed to zero slowly over 10 ns. **Conduction events were counted after excluding the first 10 ns of equilibration.**

Because the multiple simulations underwent ion dynamics that are uncorrelated with the initial placement, we feel that further simulations with other starting configurations are not needed for the purpose of proving that the channel is capable of supporting ion conduction.

2. - More importantly, if I understand correctly, the starting configuration was different for the simulations in low K<sup>+</sup>. This is not explicitly stated in the Methods, but looking at Figures 1 and S6, it seems that the simulations at low K<sup>+</sup> were initialized without ions in S1, S2 and S3. The absence of ions in these sites is going to cause a distortion in the structure of the selectivity filter that might justify the lack of conduction events. I think that the two sets of simulations (using restraints to preserve respectively the high/low K<sup>+</sup> structures) should be initialized in the same way. Otherwise, it is hard to know if the difference in conductance is due to the alternative restraints adopted or to the different initial configurations.

The sets of high K<sup>+</sup> (conducting) and low K<sup>+</sup> (non-conducting) state simulations-were initialized in exactly the same way, with five ions initially held in S0-S4. We apologise for not making this clearer in the manuscript and have modified the methods to remove this confusion. (page 23, line 35)

Simulations starting with **either** the high-K structure **or low-K structure** were similar to those described above, ...

To make this clearer, we have included additional panels in the supplementary figure (now Supplementary Fig S7) that highlight the ion equilibration period for both lowK and highK structures to show that both simulations started with 5 ions. In the case of the low-K structure (Supplementary Fig

S7E; with zoomed graph in Supplementary Fig. S7F), the unstable ions instantly shift, with one ion leaving immediately and two others leaving the filter within 0.2ns, despite strong restraints. This reflects the highly repulsive nature of the flipped V625 backbone, presenting amide N-H groups to the cations inside the filter. Shortly after release of all restraints, no ions remained in the filter. This is distinct from the conducting simulations (highK structure with V625 carbonyls pointing inwards), where the 5 ions remain in the filter during the equilibration period, but the outermost ions leave immediately after the final restraints are released with the filter then containing 2-3 ions (Supplementary Fig 7G). The redistribution of ions in the initial period were not included in our counts of ion conduction events. The additional information included in the legend to supplementary Fig S7 is:

**E.** The 10 ns equilibration period of the nonconducting replica 1, plus another 10 ns of the production run (full production MD in panel A). Restraints on the ions inside the filter are decoupled slowly over the first 10 ns. **F.** First 1 ns of the equilibration phase from E, showing that, in the low-K filter, the ions leave the selectivity filter instantly. **G.** The 10 ns equilibration period of the conducting replica 1 where the selectivity filter ion restraints are slowly decoupled, plus another 10 ns of the production run. The 5 ions remain in the filter during the equilibration period, but the outermost ions leave immediately after the final restraints are released with the filter then containing 2-3 ions. The redistribution of ions in the initial period were not included in our counts of ion conduction events.

3. - The set of initial ion configurations used to explore the effect of K<sup>+</sup> ions on the structure of the selectivity filter misses important configurations with ions in adjacent binding sites. Configurations with ions in S3 and S2 were observed to be the most stable ones in several potassium channels, including hERG [J Chem Inf Model. 2023 Jan 9;63(1):251-258], in simulations with both AMBER and CHARMM force fields [J Am Chem Soc. 2021 Aug 11;143(31):12181-12193][ J Chem Theory Comput. 2023 May 9;19(9):2574-2589]. I think that these ion configurations should be included in the set, also considering that the contemporary presence of ions in S2 and S3 is likely to impact on the flipping properties of V625.

For this initial examination of the effects of ion binding on filter dynamics, we chose to include ions either in individual binding sites (to probe the apparent control that ion binding to particular sites has on filter dynamics) or in “canonical” multi-site configurations (S0/S2/S4, S1/S3) that might help better pin down carbonyls directed inwards. The primary reason for choosing this particular set of simulations was so that we could compare our results directly to the previous simulations for KcsA (Berneche & Roux 2005) and MthK (Boiteux PNAS 2020). However, we recognised that it is important to study filter dynamics in the presence of the equilibrium distribution of ions, hence the inclusion of the comprehensive REST2 simulations. The REST2 simulations enable thorough equilibrium sampling of ion and protein configurations (paragraph starting line 24 on p8). Because the REST2 simulations cover all ion configurations, and serve a different purpose to the initial constrained ion survey, we do not feel additional simulations in the initial survey are necessary.

Nevertheless, we agree with the reviewer that it is worth mentioning the presence of the S2/S3 ion configurations in the legend to supplementary Fig S9C (previously suppl Fig 8) and in the results (see details below).

#### Legend for Supplementary Figure 9

When all four V625 carbonyl oxygens were directed inward (13 % of the time; shown in red), there was on average 2.7 ions in the selectivity filter. Whilst we observed the canonical S2/S4 and S0/S2/S4 configurations, more commonly we observed ions in S2/S3, S0/S2/S3 or S1/S2/S3.

Results (page 10, lines 4-9)

There were frequent movements of ions between sites, and in addition to the canonical configurations we also observed ions present in S2 and S3 simultaneously, further constraining backbone carbonyl groups inside the filter (Supplementary Fig 9C). However, given evidence for the effect of force field on propensity for channel closure<sup>33</sup>, the distribution of ion configurations and their effects on filter structure may differ in other models.

To specifically address the reviewers concern re: the impact of ions in S2 and S3 on the flipping properties of V625, the 2-dimensional free energy plots for Ser620 side chain interactions with V625 Carbonyl, Y616 carbonyl and F627/G626 amides as a function of rotation of the V625 carbonyl were obtained from the REST2 simulations (which includes S2/S3 configurations). Please note that these plots have been recalculated using MBAR (see response to point 4 below and see new Figure 4C-F). Qualitatively, the 2D PMF plots in Figure 4C-F are very similar to the plots obtained from the constrained ion MD simulations (supplementary Fig 11) which suggests that there is a comparable coverage of protein conformational dynamics in the two distinct data sets.

Finally, we acknowledge that recent work has emphasised the force field dependence of ion distributions in ion channel simulations. We agree that this is something that should be pursued in more detail for HERG channels in future studies and have acknowledged this in the limitations section of the discussion (page 17, lines 3-5)

In future studies, it would also be important to consider the impact that using different force fields in MD simulations could have on distribution of ion configurations and their effects on filter structure<sup>33</sup>.

4. - In previous MD simulations of hERG with the CHARMM force field [Proc Natl Acad Sci. 2020 Feb 11;117(6):2795-2804][Sci Adv. 2021 Jan 29;7(5):eabd6203] the selectivity filter closes in a few hundreds of nanoseconds. Closure of the selectivity filter in this time scale is a known characteristic of the CHARMM force field [J Chem Theory Comput. 2020 Nov 10;16(11):7148-7159]. Closure events do not seem to take place in the solute tempering simulations presented here; otherwise, I would expect a completely different free energy profile for the permeating ions. It would be interesting to include a comment about this difference with previous literature in the manuscript.

It is important to note that the final data from our REST2 simulations that was shown in the original manuscript (Figure 3C) included all ion and protein configurations, both conducting and nonconducting, so one cannot assume that there were no closure events included. In our revised analyses (Figure 3D, revised manuscript), we have decomposed according to the number of V625 flips, 0-4. With MBAR we achieve good sampling of wells and barriers for 0-3 flips, but only capture the low free energy regions with 4 flips. The free energy wells for S1, S2 and S3 are 3-4 kcal/mol deep when 0, 1, or 2 V625 backbone carbonyls are flipped, but become significantly destabilised when 3 or 4 V625 backbone carbonyls are flipped, suggesting these cases may relate to the non-conducting form of the channel, and have been sampled.

In the revised manuscript we have included a more thorough analysis of the REST2 simulations which has enabled us to calculate the free energy profiles for 0, 1, 2, 3, and 4 flipped V625 backbone carbonyls (new Figure 3D, revised manuscript). When all four V625 backbone carbonyls are flipped we do not observe transitions between S1-S2, S2-S3 or S3-S4 and the free energy well depths for ion occupancy of these sites are very low. Conversely, the free energy wells for S1, S2 and S3 are 3-4

kcal/mol when 0, 1, or 2 V625 backbone carbonyls are flipped and only become significantly destabilized when 3 or more V625 backbone carbonyls are flipped. We have modified text on page 10 to highlight this point. Furthermore, that we did not observe sufficient sampling of the free energy barriers to ion movement when all four V625 backbone carbonyls were flipped suggests that this configuration is indeed non conducting.

These points are made in the new manuscript (see page 10, lines 11-19):

We next analyzed the free energy profile of ion distribution in the filter according to the number of flipped V625 backbone carbonyls (Fig 3D). Using Multistate Bennett Acceptance Ratio (MBAR)<sup>34</sup>, we exploit the sampling in all 16 REST2 replicas to obtain an optimal estimate of free energies in the unscaled replica. We achieve good sampling of wells and barriers for 0-3 flips, but only capture the low free energy regions with 4 flips. The free energy wells for S1, S2 and S3 are 3-4 kcal/mol when 0, 1, or 2 V625 backbone carbonyls are flipped, but become significantly destabilized when 3 or 4 V625 backbone carbonyls are flipped. This suggests that 0,1 or 2 flipped V625 backbone carbonyls are consistent with a conductive conformation whilst 3 or 4 flipped V625 backbone carbonyls may relate to the non-conducting form of the channel.

On the broader point raised by the reviewer about the force field dependence of ion-protein interaction energies, we acknowledge that this is a limitation that warrants further investigation in future studies. We have mentioned this in the discussion of the REST2 analyses (see page 10, lines 7-9):

However, given evidence for the effect of force field on propensity for channel closure<sup>33</sup>, the distribution of ion configurations and their effects on filter structure may differ in other models.

And in the limitations section of the discussion (page 17, lines 3-5):

In future studies, it would also be important to consider the impact that using different force fields in MD simulations could have on distribution of ion configurations and their effects on filter structure<sup>33</sup>.

## REVIEWER COMMENTS

Reviewer #1 (Remarks to the Author):

I appreciate the efforts by the authors to respond to my questions. I think they have done an appropriate job of better pointing out caveats of the modelling and alternative explanations based on experimental data. This has somewhat reduced the potential definitiveness of the proposed mechanism, but I have no further points to make. Congratulations!

Reviewer #2 (Remarks to the Author):

My concerns have been addressed.

Reviewer #3 (Remarks to the Author):

The authors have adequately addressed my comments, but there are a few additional points to consider. Once these points are addressed, I believe this manuscript will be suitable for publication.

[Additional point #1 in "Supplementary Material"]

In Supplementary Figure S2 E(i), E(ii), E(iii), and E(iv), the phase-randomized FSC curves (red curves) indicate that the masks used in the post-processing jobs were too tight and potentially resulting in an over- or under-estimation of the FSC resolution. Upon reviewing the masks provided by the authors, it appears that the soft-edge widths of these masks are very narrow (perhaps around 6 pixels).

As you are aware, ideally, the slope of the red curve should be as steep as possible, and the first zero-crossing of the red curve must be much lower than the 0.143 FSC resolution indicated by the "blue" curve. Consequently, Supplementary Figure S2 E(i) and E(ii) fail to meet these criteria, E(iii) raises suspicion, while E(iv) is acceptable.

Therefore, the authors must redo these post-processing jobs using masks with a wider soft-edge widths.

Although there is currently no clear community consensus of how steep the slope should be and how low the first zero-crossing should be, I recommend the following:

- (1) Use soft-edge widths wider than 10 pixels for masks.
- (2) Ensure that the first zero-crossing of the red curve is lower than the 0.143 FSC resolution of the "green" curve. Instead of 0.143, I personally use the 0.5 FSC resolution of "green" curve to be safe.

Additionally, please include descriptions of the curves corresponding to each color in these panels.

[Additional point #2 in "Supplementary Material"]

There is a discrepancy in the map-to-model FSC resolution values of high-K with C1 symmetry between Supplementary Figure S2 F(iii) (3.6 Å) and Supplementary Table 1 (3.8 Å).

Reviewer #4 (Remarks to the Author):

I really appreciated the revised version of the manuscript, and the efforts put by the authors in

replying to my comments. In the current version of the study, the model that is proposed for the transition between the conductive and the non-conductive state requires the switching of at least 3 V625 carbonyls. This model answers to my previous concern about the low-energy barrier for a single V625 flipping. However, a similar concern applies now to the flipping of 3 or 4 V625 carbonyls. The simulations presented in this study do not prove that the 4 flipped state is a free energy minimum separated from the local free energy minimum that corresponds to the conductive state by energy barriers that are compatible with inactivation. In the authors' response, it is stated that a more extensive analysis of the impact of 1,2,3 & 4 flipped V625 carbonyls on the stabilization of the non-conductive state versus conductive states is beyond the scope of the present study but should be pursued in future studies. I totally understand this approach, but to avoid misunderstandings I think that a few changes should be implemented. Figure 6 is presented as a model for transition from a conductive to a non-conductive selectivity filter. However, the non-conductive state is labelled as "I", and referred to as "inactivated" in the figure legend. It is easy to make confusion about what is proposed with this model. As this is presented as an hypothesis, I think that it is fine (almost unavoidable) to name the final state as an inactivated state. But in this case, it is important to state among the limitations of the study that the impact of the flipping on the stabilization of the non-conductive versus conductive state still needs to be proved, and consequently that the link between the non-conductive state and the inactivated state is an hypothesis. This is a different (and preceding) limitation with respect to the one discussed in the text about what is the rate limiting step, as there might be no rate-limiting step compatible with inactivation between the conductive and the non-conductive state. For the same reason I suggest the following changes:

- The abstract concludes as: "Our model represents a new mechanism by which ion channels fine tune their activity that explains the uniquely rapid inactivation kinetics of HERG". I think that this last sentence should be rephrased in more cautious terms.

- On page 9 line 202, the V625 flipped state should not be referred as "inactivated state, Fig. 3C".

On a second topic, I do not fully agree with the conclusion that the PMF shown in Figure 3D suggest that 0, 1, or 2 flipped V625 carbonyls are consistent with a conductive conformation while 3 or 4 might relate to a non-conductive form. While it is true that the energy wells are 3-4 kcal/mol higher in the 3 flipped state, binding sites are still there, and moreover, if I compare the energy barrier between S2 and S3 in the red (0 flip) and purple (3 flips) lines, the barrier with 3 flips seems even lower than the one in 0 flipped state. What I'd conclude from these PMFs is that 0, 1, 2, or 3 flipped V625 carbonyls are consistent with a conductive conformation, while 4 might relate to a non-conductive form, in agreement with the fact that it was not possible to sample the transition state for the 4 flipped configuration. If this is not the case and I am misinterpreting the figure, I suggest to modify Figure 3D for better highlighting the differences.

### **Reviewer #1 (Remarks to the Author):**

I appreciate the efforts by the authors to respond to my questions. I think they have done an appropriate job of better pointing out caveats of the modelling and alternative explanations based on experimental data. This has somewhat reduced the potential definitiveness of the proposed mechanism, but I have no further points to make. Congratulations!

### **Reviewer #2 (Remarks to the Author):**

My concerns have been addressed.

### **Reviewer #3 (Remarks to the Author):**

The authors have adequately addressed my comments, but there are a few additional points to consider. Once these points are addressed, I believe this manuscript will be suitable for publication.

[Additional point #1 in "Supplementary Material"]

**In Supplementary Figure S2 E(i), E(ii), E(iii), and E(iv), the phase-randomized FSC curves (red curves) indicate that the masks used in the post-processing jobs were too tight and potentially resulting in an over- or under-estimation of the FSC resolution. ... Consequently, Supplementary Figure S2 E(i) and E(ii) fail to meet these criteria, E(iii) raises suspicion, while E(iv) is acceptable.... the authors must redo these post-processing jobs using masks with a wider soft-edge widths ... I recommend the following: (1) Use soft-edge widths wider than 10 pixels for masks. (2) Ensure that the first zero-crossing of the red curve is lower than the 0.143 FSC resolution of the "green" curve. Instead of 0.143, I personally use the 0.5 FSC resolution of "green" curve to be safe.**

We have redone post-processing jobs using masks with 12 pixels soft edge. First zero crossing of all phase randomized masked maps are below 0.143 FSC of the unmasked maps. The gold-standard resolution remain unchanged for all structures with this new post-processing.

The updated mask, post-processed maps, FSC curves, and refined PDBs have been uploaded to wwPDB. The Model-map FSC plots in supplementary figure S2E have also been updated.

**Additionally, please include descriptions of the curves corresponding to each color in these panels.**

The following description has been added to the figure legend for Figure S2:

(Black: corrected map. Blue: masked maps. Red: phase randomized masked maps. Green: unmasked maps)

[Additional point #2 in "Supplementary Material"]

**There is a discrepancy in the map-to-model FSC resolution values of high-K with C1 symmetry between Supplementary Figure S2 F(iii) (3.6 Å) and Supplementary Table 1 (3.8 Å).**

This value should be 3.6 Å. The mistake in Supplementary Table 1 has been fixed.

### **Reviewer #4 (Remarks to the Author):**

I really appreciated the revised version of the manuscript, and the efforts put by the authors in replying to my comments. In the current version of the study, the model that is proposed for the transition between the conductive and the non-conductive state requires the switching of at least 3 V625 carbonyls. This model answers to my previous concern about

the low-energy barrier for a single V625 flipping. However, a similar concern applies now to the flipping of 3 or 4 V625 carbonyls. The simulations presented in this study do not prove that the 4 flipped state is a free energy minimum separated from the local free energy minimum that corresponds to the conductive state by energy barriers that are compatible with inactivation. **In the authors' response, it is stated that a more extensive analysis of the impact of 1,2,3 & 4 flipped V625 carbonyls on the stabilization of the non-conductive state versus conductive states is beyond the scope of the present study but should be pursued in future studies. I totally understand this approach, but to avoid misunderstandings I think that a few changes should be implemented.** Figure 6 is presented as a model for transition from a conductive to a non-conductive selectivity filter. However, the non-conductive state is labelled as "I", and referred to as "inactivated" in the figure legend. It is easy to make confusion about what is proposed with this model. As this is presented as an hypothesis, I think that it is fine (almost unavoidable) to name the final state as an inactivated state. But in this case, **it is important to state among the limitations of the study that the impact of the flipping on the stabilization of the non-conductive versus conductive state still needs to be proved, and consequently that the link between the non-conductive state and the inactivated state is an hypothesis.** This is a different (and preceding) limitation with respect to the one discussed in the text about what is the rate limiting step, as there might be no rate-limiting step compatible with inactivation between the conductive and the non-conductive state.

To reduce some of this confusion we have modified Figure 6 to label the conducting and non-conducting states as C and NC and we have modified the legend accordingly:

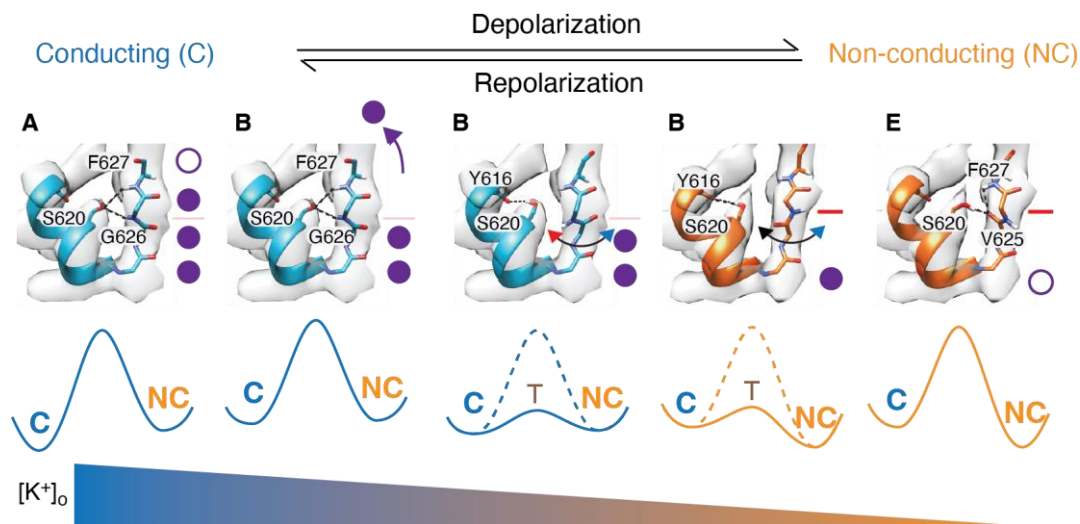


**Figure 6: Proposed model for transition from conducting to non-conducting selectivity filter.** Cryo-EM maps of the selectivity filter obtained from the high-K structure (panels **A-C**) and low-K structure (panels **D-E**) with superimposed protein structures obtained from snapshots of the MDFF fits to the high-K (blue) or low-K (orange) cryo-EM maps. Stylized free energy diagrams for the transition from the conductive (C) to non-conductive (NC) state, via a transition state (T) are shown below each panel. Interactions stabilizing each state are highlighted as dashed lines in each panel (**A,B**: S620 – F627/G626, **C,D**: S620 – Y616; **E**: S620-V625). **The transition from conducting to non-conducting states** is initiated by K<sup>+</sup> ions leaving the upper filter, **B**. The energy barrier for movement of ions between S3 and S2 (faint pink line, panels **A,B,C**) is increased when all four V625 backbone carbonyls are flipped (red line in panels **D,E**). The gradient for [K<sup>+</sup>]<sub>o</sub> indicates that the conductive state is favored at high [K<sup>+</sup>]<sub>o</sub> and the non-conducting state is favored at low [K<sup>+</sup>]<sub>o</sub>. A movie depicting the transition from the conductive to non-conductive states is shown in Supplementary Movie 1.

We have also modified the limitations section which is described in more detail in response to the points below

- **The abstract concludes as: “Our model represents a new mechanism by which ion channels fine tune their activity that explains the uniquely rapid inactivation kinetics of HERG”. I think that this last sentence should be rephrased in more cautious terms.**

We have modified the last sentence of the abstract from:

Our model represents a new mechanism by which ion channels fine tune their activity and can explain the uniquely rapid inactivation kinetics of HERG

to:

Our model represents a new mechanism by which ion channels fine tune their activity **and could** explain the uniquely rapid inactivation kinetics of HERG

- **On page 9 line 20, the V625 flipped state should not be referred as “inactivated state, Fig. 3C”.**

We have modified this sentence as follows

Page 9, lines 28-29:

“at  $\Psi \sim -50^\circ$  (V625 carbonyl non-flipped) and  $\Psi \sim 70^\circ$  (flipped V625 carbonyl, Fig 3C)”

On a second topic, I do not fully agree with the conclusion that the PMF shown in Figure 3D suggest that 0, 1, or 2 flipped V625 carbonyls are consistent with a conductive conformation while 3 or 4 might relate to a non-conductive form. While it is true that the energy wells are 3-4 kcal/mol higher in the 3 flipped state, binding sites are still there, and moreover, if I compare the energy barrier between S2 and S3 in the red (0 flip) and purple (3 flips) lines, the barrier with 3 flips seems even lower than the one in 0 flipped state. What I'd conclude from these PMFs is that 0, 1, 2, or 3 flipped V625 carbonyls are consistent with a conductive conformation, while 4 might relate to a non-conductive form, in agreement with the fact that it was not possible to sample the transition state for the 4 flipped configuration. If this is not the case and I am misinterpreting the figure, I suggest to modify Figure 3D for better highlighting the differences.

We agree with the reviewer re: 0, 1, or 2 flipped V625 carbonyls being consistent with a conductive conformation, whilst the 4 flipped V625 carbonyls state is consistent with a non-conductive conformation. We also agree that we cannot make a definitive statement about what the 3 flipped state represents. The depth of the wells at S1, S2, and S3 are not as deep for 3 flipped compared to 0,1, or 2 flipped states, and indeed more closely resembles the 4 flipped state, consistent with this representing a non-conducting state. However, the barriers for transitions between S1-S2, S2-S3 and S3-S4 for the 3 flipped state are similar to those for the 0,1, or 2 flipped states, which is different to that for the 4 flipped state. We accept that whether the 3 flipped state is conducting or non-conducting remains unresolved and needs further investigation (as agreed by the reviewer). To clarify this point, we have modified the text as follows:

page 13, lines 23-26:

“The non-conducting state is stabilized by the flipped V625 backbone carbonyl binding to the S620 side chain and **at least three, and possibly all four**, V625 backbone carbonyls need to be maintained in the flipped state for the channel to become non-conductive (Fig 3D)”

Page 16, lines 20-21:

**from the REST2 simulations we suggest that at least 3, and possibly all four, V625 backbone carbonyls must be stabilized in the flipped state for the channel to become non-conducting.**

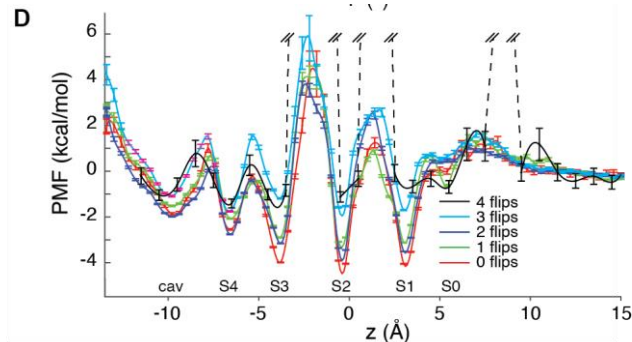
Page 17, lines 4-7:

**Furthermore, whilst the REST2 simulations strongly suggest that when all four V625 carbonyls are stabilised in the flipped state the channel is non-conducting, we cannot**

rule out the possibility that only three flipped V625 carbonyls may be sufficient to stabilise the non-conducting state.

We have also changed the legend for Figure 6 as follows:

The energy barrier for movement of ions between S3 and S2 (pink line, panels **A,B**) is increased when all four V625 backbone carbonyls are flipped (red line in panels **D,E**) As we now mention the uncertainty about three versus four flipped state in the limitations section we are happy to focus on the four flipped state in the model figure as that is what is most clear from the data shown in Figure 3D. Lastly, on reviewing Figure 3, we felt that the pink and red lines in panel 3D were hard to distinguish so we have changed the line for the three flipped state from pink to cyan:



## **REVIEWERS' COMMENTS**

Reviewer #3 (Remarks to the Author):

All my concerns have been adequately addressed by the authors, and I have no further points to make. I believe this manuscript is suitable for publication.

Reviewer #4 (Remarks to the Author):

All my comments have been addresses. Congratulations for the excellent work.